Response to Review Comments for *A Decade of GOSAT Proxy XCH₄ Observations*

Firstly, we would like to express our gratitude to the editor and reviewers for providing a thorough review of our paper. We appreciate their efforts, especially in these difficult times.

This document contains our point-by-point response to the review comments including a list of all relevant changes made in the manuscript and a marked-up manuscript version identifying the changes made.

1 Response to RC1 Review Comments

(Original Comment, Our Response, New Manuscript Text)

1. Abstract: I think it is important to mention that TM5 assimilates NOAA background data, because it is in fact unclear how much of the comparison to GOSAT reflects consistency of GOSAT with NOAA vs. with the TM5 methane budget and transport. This lack of clarity should be acknowledged, not necessarily in the abstract but surely in the text (it's kind of there, could be made stronger).

To explain, our comparisons to model data are to ensure that we are in broad agreement with simulations at the level where further scientific investigation (e.g. flux inversions) would make sense to conduct. Comparisons to a free-running unconstrained CH₄ simulation would likely show offsets/differences and it would then be unclear if these were due to the satellite data or the model simulation. By having good overall agreement to both TCCON and the NOAA-constrained model simulations, we believe this indicates the utility of our data for use in such studies. We will add additional clarification to the manuscript text in Section 7.

We have chosen to compare against model simulations that are both widely used within the community and that have already assimilated NOAA surface measurements. The reasoning for this is that any overall differences as might be seen from free-running model simulation are removed and we can clearly state the consistency of our dataset with the NOAA network. By proving good overall agreement to both TCCON measurements (Section 5) and the NOAA-constrained model simulations we believe this indicates the utility of our data for use in further scientific analysis.

2. Page 4, around line 5: mention that GOSAT also operates in target mode. Hasn't it been doing so increasingly in recent years? This provides additional info but also disrupts the time series. I also don't think that the time series have been kept at consistent locations for the 10 years – they seem to shift. But the authors would know for sure.

We have included an additional figure which we believe is informative and addresses this point. The GOSAT measurement strategy/capability has indeed changed over time, however we do not believe that the timeseries has been "disrupted" in any significant way. As discussed in RC3, the switch to the secondary pointing mechanism has had an effect on the coverage, extending the ocean glint range and the number of target observations. We discuss this in the manuscript and highlight it with Figure 10. This additional figure (*Response Supplement Figure 1*) provides further details, particularly relating to the 3-point repeat grid vs target observations. We have added this to a new appendix section detailing the sampling/measurement details and also included a second figure (*Response Supplement Figure 2*) that we believe is informative.

This section provides details on how the GOSAT measurement strategy has evolved over time. GOSAT initially operated primarily on a regular 5-point grid, revisiting the same grid point. This changed over time to a 3-point grid in order to reduce pointing uncertainty at the extreme angles when using the primary pointing mechanism. However, one consequence of a regular grid is that this resulted in a limited number of observations over some regions, especially islands, where the regular grid point would fall over the ocean. Thanks to the switch to the secondary pointing mechanism, several changes to the sampling strategy were possible.

Firstly, GOSAT is now capable of targeting more specifically and "follows" coastlines in a more efficient manner. The example in Figure 1 shows the change in sampling location over Indonesia, contrasting 2011 to 2017. Although the exact same grid location is not revisited in the same way, overall there are both more successful measurements and a better geographic coverage.

Secondly, GOSAT is now capable of a wider pointing range and subsequently, the latitudinal range of ocean sun-glint observations have been extended (as observed in Figure 10). Figure 2 provides example comparisons of the measurement density over Australia between the start of the mission (2009-2010) when the instrument was primarily operating in 5-point grid mode to the latter years (2018-2019) where the instrument is operating in 3-point grid mode, with extended latitudinal sun-glint coverage.

While we do not believe that these changes are detrimental to the continued consistency of the timeseries of GOSAT observations, we do feel that it is worth noting as they may have an impact (positively or negatively) on specific applications that a user may wish to use the data for, hence the reason for highlighting them here.

3. Page 5, line 26: Maasakkers et al. 2019 comment on OH variability but attribute most of the 2010-2015 GOSAT trend to tropical wetlands and livestock.

We've adjusted this reference in the manuscript to cover both aspects.

4. Page 6, Section 4: I'm surprised that the role of aerosols (e.g., dust plumes) is not mentioned anywhere in this section.

We have added in explicit mention of aerosol and why the proxy retrieval method mitigates a lot of the aerosol considerations that would be required for the "full physics" algorithm.

This means that moderate aerosol scattering does not adversely impact upon the retrieval, resulting in a higher number of high-quality XCH_4 observations compared to the full physics approaches where much stricter post-filtering are often required. This is especially useful over the tropics, where moderate aerosol or cirrus effects can limit the coverage of full-physics methods but affect the proxy approach far less severely.

5. Page 9, Section 7: see comment in the abstract. In comparisons over broad regions like in Figure 12 one wonders how much of the fit is due to the assimilation of NOAA data in the model.

See response above for abstract comment.

6. Page 21, line 12: two good references for model biases in the stratosphere are Patra et al. ACP 2011 and Saad et al. ACP 2016.

We will include these in the manuscript.

7. Page 21, line 14: Turner et al. ACP 2015 also have a quadratic polynomial correction for model-GOSAT bias vs latitude.

Noted. We will include reference to this in the appropriate section.

2 Response to RC2 Review Comments

(Original Comment, Our Response, New Manuscript Text)

Two main comments: First, why have there been 9 Versions of the GOSAT XCH_4 proxy product? A table documenting the version, release date, and changes, would be very helpful.

We have now included a detailed breakdown of the previous versions of the UoL GOSAT Proxy XCH_4. We initially omitted this as we wanted to focus on v9.0 but we accept that this is a useful table and puts the current data in context.

Table 2 (*Response Supplement Table 2*), provides details of the evolution of the University of Leicester GOSAT Proxy XCH_4 data product. Entries include the version number, the project that the data was generated for, the version of the GOSAT L1B data used, the time period covered by the data, whether ocean sun-glint data was generated, comments relating to changes/updates from previous versions and peer-reviewed publications that we are aware of that used the data. For the ESA GHG-CCI project, we also indicate which versions were officially delivered as part of the Climate Research Data Packages through the project. All Copernicus C3S versions were delivered to the Copernicus Climate Data Store.

In addition, there is no forward looking discussion..., what can we expect for version 10 and upward? What remains or is needed in future, e.g., how will constellations be integrated, or GOSAT2. What is mission lifetime for GOSAT given degradation of instruments, orbit, etc.

We have also included a statement regarding the future evolution of the product. However, we do not feel it is our place to comment directly on the future of the GOSAT mission itself as that is the responsibility of JAXA and we would not want our response to be minconstrued as any sort of official position.

Despite GOSAT-1 having a planned mission lifetime of 5 years, it continues to successfully perform measurements 11 years after launch. GOSAT-2 was launched in October 2018 (Suto et al, 2020) and will continue the legacy of the GOSAT-1 mission. GOSAT-2 offers several opportunities for development related to the dataset we describe here. Primarily, it ensures that should GOSAT-1 cease operation, the valuable decade-long timeseries of observations can continue to be extended via GOSAT-2. With a significant overlap in time between the two missions, consistency between the two missions can be assured, albeit with significant future work/development.

In addition, GOSAT-2 has additional capabilities, namely the possibility of measuring carbon monoxide (CO). By measuring CO_2, CH_4 and CO simultaneously from the same instrument, GOSAT-2 would allow the extension of studies examining biomass burning combustion, leading to constraints on fire emission ratios as have been performed previously for GOSAT-1 (Ross et al., 2013; Parker et al., 2016).

For the presented v9, a table summarizing key components is needed, such as spatial and temporal parameters, overpass time, accuracy, etc. Currently, the reader has to dig around for this key information

Table summarising product characteristics has been included - (*Response Supplement Table 1*)

Table 1 summarises the key characteristics of the University of Leicester GOSAT Proxy XCH_4 data, including the spatial and temporal extent that the dataset covers, the total number of measurements and their evaluation against TCCON.

Introduction - Mention/acknowledge there is also GOSAT-2 - Mention the nickname, IBUKI

We have included both of these points either here or above.

GOSAT is nicknamed *"Ibuki"*, meaning *breath* in Japanese, highlighting that its mission involves monitoring the breathing of the planet, through measurement of the carbon cycle.

Section 2.0: - What were the original measurement requirements – please list these as they provide a context for how well this product performs.

We have quoted the original measurement requirements as outlined in Kuze et al., 2009. Furthermore, we also refer to the User Requirements developed during the ESA CCI project.

Kuze et al. (2009) state a target relative accuracy of 2% for CH_4 over 3 month averages at 100-1000 km spatial scales. The ESA GHG-CCI User Requirements Document (URD) specify goal (G), breakthrough (B) and threshold (T) requirements, with the goal requirements being the most stringent (Buchwitz et al, 2017). For XCH_4 precision, these values are 9, 17 and 34 ppb respectively. We discuss in Section 5 how we exceed these breakthrough requirements.

The single measurement precision of 13.72 ppb comfortably exceeds the precision breakthrough requirement of 17 ppb (Buchwitz et al, 2017) indicating that it "would result in a significant improvement for the targeted application"

Where is the Project Science Office located – mention this as its important to acknowledge the primary data management group.

We are extremely grateful for the help and support we have received from the entire GOSAT project. We acknowledge this in the acknowledgements section. We have also reached out to the GOSAT Project Office directly to ensure that they are happy with the current statement and they have confirmed that they are.

Section 3.2 - Refer to Sentinel-5 nomenclature when TROPOMI is mentioned - Also, PRISMA and HISUI should be mentioned for their CH_4 retrieval potential.

...continue to be performed from new missions such as TROPOMI onboard Sentinel 5-Precursor and...

We have included menton of PRISMA and HISUI in the forward looking discussion.

A strong focus of future CH_4-measuring satellites will be to examine anthropogenic emission sources at very high spatial resolution (e.g. PRISMA (Stefano et al, 2013); HISUI (Matsunaga et al., 2018); ENMAP (Guanter et al., 2015)), particularly relating to monitoring of the oil and gas industry. However, many scientific challenges and questions remain regarding the long-term CH_4 behaviour and the response to a changing climate. For this reason, a long-term, consistent climate-ready data record as we present here is of continued importance.

Typo – systemtically

Fixed in manuscript.

Fig 10 – given how small these figures are, and the size of the grid cell used to represent the XCH_4 concentration, the images give the reader a false sense of coverage. I would recommend a new, similar paneled, figure that has something like # of observations, or the cloud mask, to highlight the geographic coverage issue more clearly.

Additional figure *Response Supplement Figure 3* showing number of observations. This has been incorporated into the new appendix section detailing the sampling/measurement details.

Figure 3 shows the number of successful GOSAT XCH_4 measurements per 2° latitude-longitude bin for each year/season.

3 Response to RC3 Review Comments

(Original Comment, Our Response, New Manuscript Text)

Specific Comments

(1) Page 3, Line 15, "This version (ver9)" Are the full-physics and proxy algorithms updated simultaneously?

This paper deals purely with the proxy retrieval algorithm and does not relate to the full-physics algorithm at all. These algorithms are developed and processed separately, with the CH_4 full-physics being closely tied to the CO_2 full-physics.

Brief explanation of version up history and its improvements will help readers' understanding.

Please see response to RC2. We have included a detailed version history in the appendix.

(2) Page 4, Line 12, "Switch to the secondary pointing mechanism" GOSAT sampling pattern has changed since January 2015 when the unstable primary pointing mechanism has been changed. The secondary mechanism has much better performance of settling down. Both pointing fluctuation and bias had been removed. It also has wider pointing range in the along track direction. Therefore, more target observations for large emission sources have been allocated instead of grid observation with the nominal 3-point cross-track scan mode. Over the ocean, latitudinal range of glint observation has been widened. For 11-year GOSAT operation, this is the largest event that had affected the performance. Addition of description will be helpful to understand the description on Figure 4 in page 10.

We have added some of this very useful description to the manuscript text. We have also included a new appendix section and additional figures in response to the other review comments that directly relate to this topic. Please see response to RC1.

(3) Page 8, Line 21, "sounding specific a priori information" and Page 9, Line 15, "Spectral dispersion" Do authors retrieve wavelength every time by fitting GOSAT spectral to the simulation spectra?

Yes. We do state in the text that our retrieval state-vector contains components related to the spectral dispersion but we will make this more specific.

...allowing us to explicitly fit the wavelength for each spectra independently.

3.1 Technical Corrections

(1) pages 28-32, references A few discussion papers of AMTD and ACPD are referred. They seem to be reviewed and published as AMT and ACP papers.

We have updated all citations in the manuscript where a final published version of the reference has now been published.

4 Response Supplement - Additional Figures/Tables

This section contains additional figures and tables that will be included in the manuscript.
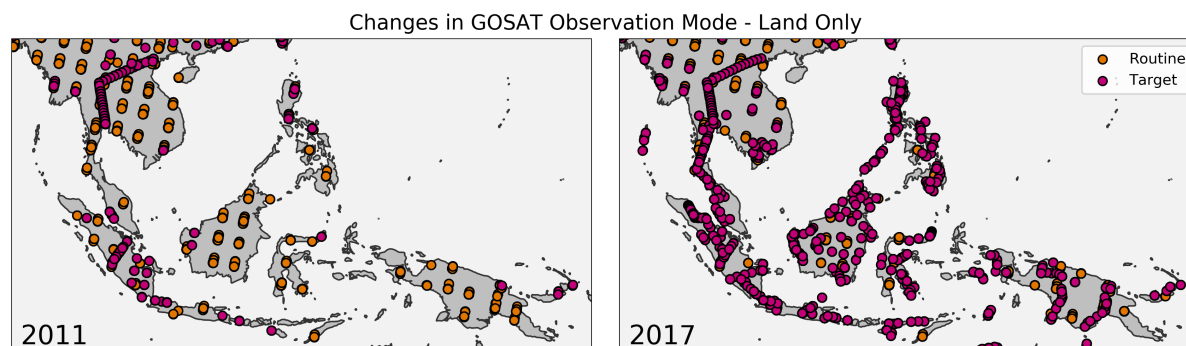

Figure 1. Figure contrasting the routine vs target observation modes for land-only measurements in 2011 and 2017 over Indonesia.
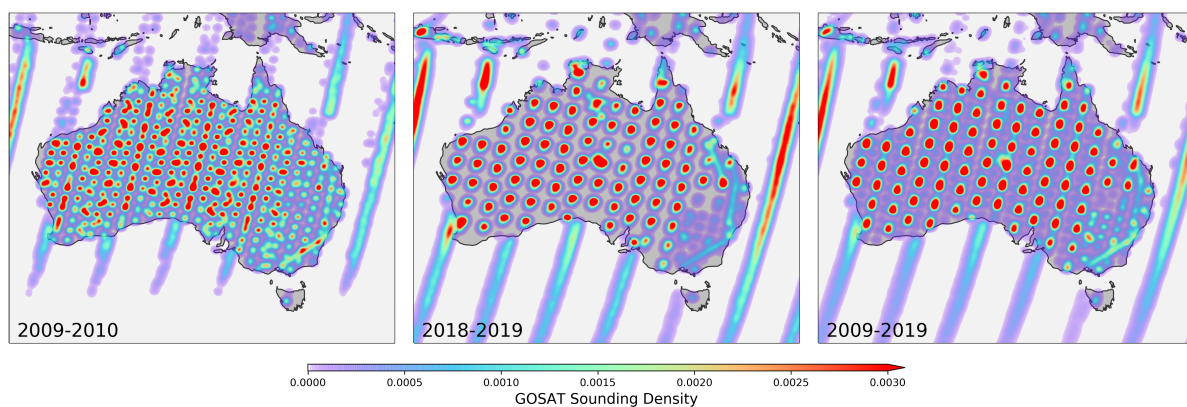

Figure 2. Figure contrasting the sampling density pattern over Australia for early in the mission versus recent years.

Attribute	Value
Temporal Extent	2009-2019
Spatial Extent	Global (56.3°S - 83.5°N)
Total Number of Measurements	4.6 million
Footprint Size	10.5km (at nadir)
Overpass Time (at Equator)	~13:00 Local Solar Time
Bias (vs TCCON)	0 ppb (after global bias correction of 9.06 ppb)
Precision (vs TCCON)	13.72 ppb

Table 1. Table summarising the key characteristics of the University of Leicester GOSAT Proxy XCH$_4$ data.

Version	Project	L1B	Time Period	Ocean?	Comments	Publications Utilising Data
1.0	NCEO	006 007	2009-2010	No	First release.	Parker et al. (2011)
2.0	NCEO	050 080 100	2009-2010	No	Development version; only processed at TCCON overpasses; new radiometric calibration for L1B from JAXA applied.	
3.0	CCI	050 080 100	2009-2010	No	First version generated as part of ESA CCI Round Robin and Algorithm Intercomparison. Improvements to surface pressure calculation taking into account instrument field-of-view. Significant speed improvements to preprocessing steps to allow multi-year processing.	
3.1	CCI	050 080 100	2009-2010	No	Incremental updates and bug fixes.	
3.2	CCI	050 080 100	2009-2010	No	Incremental updates and bug fixes. First version to be used for atmospheric inversions.	Ross et al. (2013); Fraser et al. (2013); Dils et al. (2014); Wecht et al. (2014); Cressot et al. (2014); Berchet et al. (2015); Worden et al. (2015)
4.0	CCI CRDP1	141 150 151	2009-2011	No	First version that was widely released to scientific community via CCI. Change in CO_2 model from CarbonTracker to MACCII; tightening of stratospheric covariance; spectral degradation applied as per Yoshida et al. (2013); higher resolution ERA-Interim; variable vertical grid based on tropopause height.	Fraser et al. (2014); Turner et al. (2015); Alexe et al. (2015)
5.0	CCI	160 161	2009-2013	No	Introduction of model median XCO_2 with MACCII, CarbonTracker and GEOS-Chem (as per Parker at al, 2015); CH_4 prior combines MACCII (troposphere) and TOMCAT (stratosphere); SRTM DEM used for topography; updated GOSAT L1B degradation correction based on Kuze et al. (2014).	
5.1	CCI	160 161	2009-2013	No	Resolved minor issue with uncertainty variable in 5.0.	
5.2	CCI CRDP2	160 161	2009-2013	No	Resolved minor issue with pressure weighting function In 5.1.	Parker et al. (2015); Stanevich et al. (2019, 2020)
6.0	CCI CRDP3	160 161	2009-2014	Yes	Inclusion of ocean sun-glint observations for first time.	Webb et al. (2016); McNorton et al. (2016b); Siddans et al. (2017); Feng et al. (2017); Buchwitz et al. (2017b, 2018)
6.1	CCI	160 161	2009-2015	Yes	Temporal extension of 6.0.	Ganesan et al. (2017)
7.0	CCI CRDP4	201 202	2009-2015	Yes	New L1B data and updates to CO_2 models used in ensemble for Proxy calculation.	Parker et al. (2016, 2018); McNorton et al. (2018); Sheng et al. (2018); Maasakkers et al. (2019, 2020); Lunt et al. (2019)
7.0	C3S	201 202	2009-2016	Yes	Time period extended and first delivery to C3S. No changes to processing so retained version number.	
7.1	C3S	201 202 210	2009-2017	Yes	Extension of 7.0 with updated L1B for latter years.	
7.2	C3S	201 202 210	2009-2018	Yes	Extension of 7.1 with updated L1B for latter years.	Zheng et al. (2019); Reuter et al. (2020); Yin et al. (2020); Parker et al. (2020b); Saunois et al. (2020); Tunnicliffe et al. (2020)
8.0	C3S	210	2009-2018	Yes	Internal version for testing/development of new processing pipeline.	
9.0	C3S	210	2009-2019	Yes	**The dataset described in this publication.** Fully consistent timeseries. Uses new python-based preprocessing (LRPT).	Parker et al. (2020a); Lu et al. (2020)

Table 2. Table showing the evolution of the University of Leicester GOSAT Proxy XCH_4 data product. Entries include the version number, the project that the data was generated for, the version of the GOSAT L1B data used, the time period covered by the data, whether ocean sunglint data was generated, comments relating to changes/updates from previous versions and peer-reviewed publications that we are aware of that used the data. For the ESA GHG-CCI project, we also indicate which versions were officially delivered as part of the Climate Research Data Packages through the project. All Copernicus C3S versions were delivered to the Copernicus Climate Data Store.
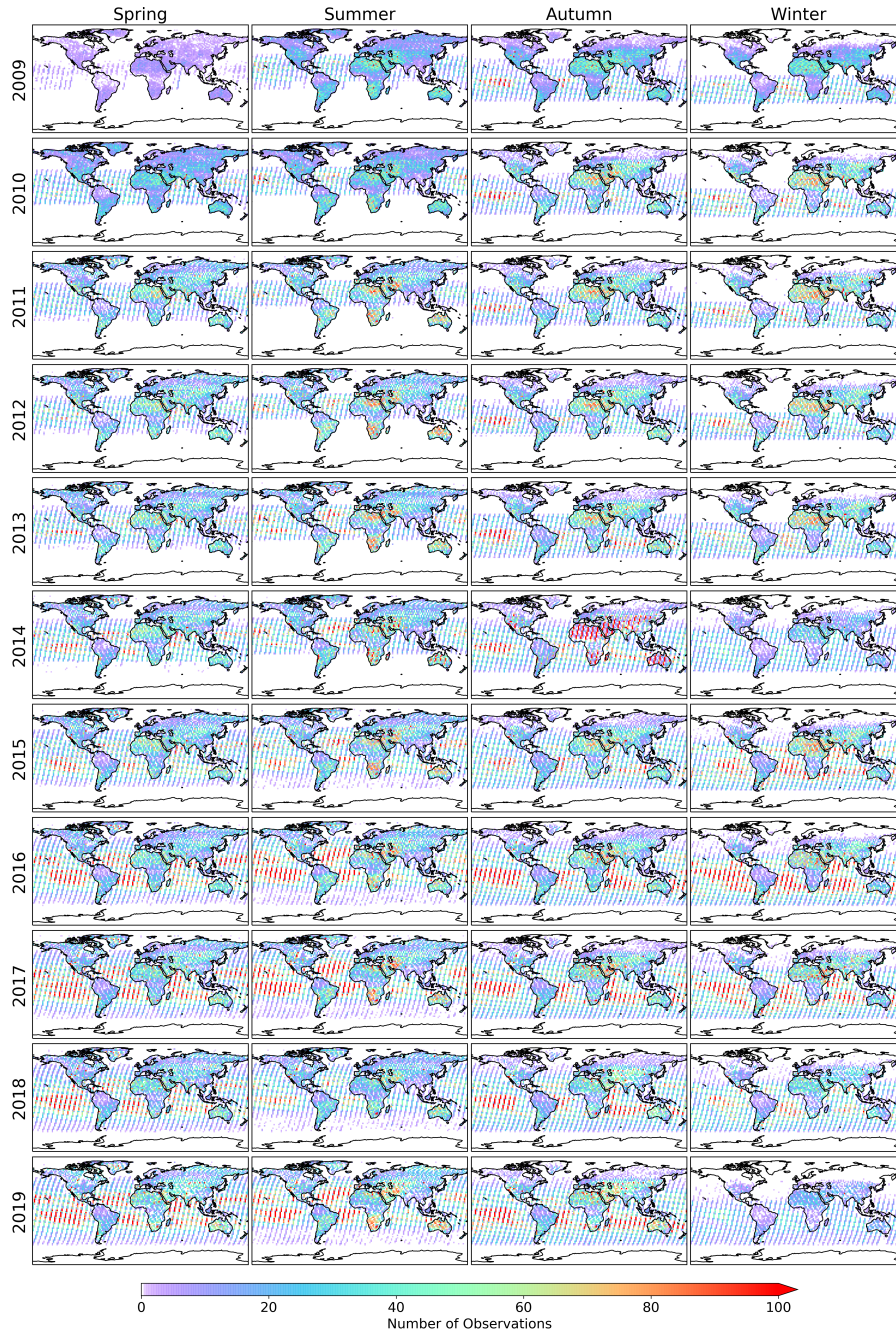
Figure 3. Figure showing the number of successful GOSAT XCH$_4$ measurements per 2° latitude-longitude bin for each year/season.

A Decade of GOSAT Proxy Satellite CH_4 Observations

Robert J. Parker[1,2], Alex Webb[1,2], Hartmut Boesch[1,2], Peter Somkuti[3], Rocio Barrio Guillo[1,2], Antonio Di Noia[2], Nikoleta Kalaitzi[1,2], Jasdeep S. Anand[2], Peter Bergamaschi[4], Frederic Chevallier[5], Paul I. Palmer[6,7], Liang Feng[6,7], Nicholas M. Deutscher[8], Dietrich G. Feist[9,10,11], David W. T. Griffith[8], Frank Hase[12], Rigel Kivi[13], Isamu Morino[14], Justus Notholt[15], Young-Suk Oh[16], Hirofumi Ohyama[14], Christof Petri[15], David F. Pollard[17], Coleen Roehl[18], Mahesh K. Sha[19], Kei Shiomi[20], Kimberly Strong[21], Ralf Sussmann[22], Yao Té[23], Voltaire A. Velazco[8], Thorsten Warneke[15], Paul O. Wennberg[18], and Debra Wunch[24]

[1]National Centre for Earth Observation, University of Leicester, UK

[2]Earth Observation Science, School of Physics and Astronomy, University of Leicester, UK

[3]Cooperative Institute for Research in the Atmosphere, Colorado State University, Colorado, US

[4]European Commission Joint Research Centre, Ispra (Va), Italy

[5]Laboratoire des Sciences du Climat et de L'Environnement, LSCE/IPSL, CEA-CNRS-UVSQ, Université Paris-Saclay, Gif Sur Yvette, France

[6]School of GeoSciences, University of Edinburgh, Edinburgh, Scotland

[7]National Centre for Earth Observation, University of Edinburgh, Edinburgh, Scotland

[8]Centre for Atmospheric Chemistry, School of Earth, Atmospheric and Life Sciences, University of Wollongong

[9]Ludwig-Maximilians-Universität München, Lehrstuhl für Physik der Atmosphäre, Munich, Germany

[10]Deutsches Zentrum für Luft- und Raumfahrt, Institut für Physik der Atmosphäre, Oberpfaffenhofen, Germany

[11]Max Planck Institute for Biogeochemistry, Jena, Germany

[12]Karlsruhe Institute of Technology, IMK-ASF, Karlsruhe, Germany

[13]Space and Earth Observation Centre, Finnish Meteorological Institute, Finland

[14]National Institute for Environmental Studies (NIES), Tsukuba, Japan

[15]Institute of Environmental Physics, University of Bremen, Germany

[16]Climate Research Division, National Institute of Meteorological Sciences (NIMS), Jeju-do 63568, Republic of Korea

[17]National Institute of Water and Atmospheric Research Ltd (NIWA), Lauder, New Zealand

[18]California Institute of Technology, Pasadena, CA 91125, USA

[19]Royal Belgian Institute for Space Aeronomy (BIRA-IASB), Brussels, Belgium

[20]Earth Observation Research Center, Japan Aerospace Exploration Agency, Japan

[21]Department of Physics, University of Toronto, Canada

[22]Karlsruhe Institute of Technology, IMK-IFU, Garmisch-Partenkirchen, Germany

[23]Laboratoire d'Etudes du Rayonnement et de la Matière en Astrophysique et Atmosphères (LERMA-IPSL), Sorbonne Université, CNRS, Observatoire de Paris, PSL Université, 75005 Paris, France

[24]Department of Physics, University of Toronto, Toronto, Canada

Correspondence: R. J. Parker (rjp23@le.ac.uk)

Abstract. This work presents the latest release (v9.0) of the University of Leicester GOSAT Proxy XCH_4 dataset. Since the launch of the GOSAT satellite in 2009, this data has been produced by the UK National Centre for Earth Observation (NCEO) as part of the ESA Greenhouse Gas Climate Change Initiative (GHG-CCI) and Copernicus Climate Change Services (C3S) projects. With now over a decade of observations, we outline the many scientific studies achieved using past versions of this data in order to highlight how this latest version may be used in the future.

We describe in detail how the data is generated, providing information and statistics for the entire processing chain from the L1B spectral data through to the final quality-filtered column-averaged dry-air mole fraction (XCH_4) data. We show that out of the 19.5 million observations made between April 2009 and December 2019, we determine that 7.3 million of these are sufficiently cloud-free (37.6%) to process further and ultimately obtain 4.6 million (23.5%) high-quality XCH_4 observations. We separate these totals by observation mode (land and ocean sun-glint) and by month, to provide data users with the expected data coverage, including highlighting periods with reduced observations due to instrumental issues.

We perform extensive validation of the data against the Total Carbon Column Observing Network (TCCON), comparing to ground-based observations at 22 locations worldwide. We find excellent agreement to TCCON, with an overall correlation coefficient of 0.92 for the 88,345 co-located measurements. The single measurement precision is found to be 13.72 ppb and an overall global bias of 9.06 ppb is determined and removed from the Proxy XCH_4 data. Additionally, we validate the separate components of the Proxy (namely the modelled XCO_2 and the XCH_4/XCO_2 ratio) and find these to be in excellent agreement with TCCON.

In order to show the utility of the data for future studies, we compare against simulated XCH_4 from the TM5 model. We find a high degree of consistency between the model and observations throughout both space and time. When focusing on specific regions, we find average differences ranging from just 3.9 ppb to 15.4 ppb. We find the phase and magnitude of the seasonal cycle to be in excellent agreement, with an average correlation coefficient of 0.93 and a mean seasonal cycle amplitude difference across all regions of -0.84 ppb.

This data is available at https://doi.org/10.5285/18ef8247f52a4cb6a14013f8235cc1eb (Parker and Boesch, 2020).

1 Introduction

Atmospheric methane (CH_4) is the second most important greenhouse gas in terms of anthropogenic climate radiative forcing (Myhre et al., 2013) with a global warming potential on a 100-year time-scale of 28-34 times that of CO_2 (Etminan et al., 2016) on a mass/mass basis. This strong warming potential, when coupled to its short lifetime relative to that of CO_2 (Prather et al., 2012) makes it of particular interest when considering rapid and achievable mitigation strategies (Nisbet et al., 2020).

Scientific debate continues on trying to explain the atmospheric CH_4 trend observed over the past couple of decades. Records from surface sites reveal a plateau from 2000 to 2007 and a resumed increase after 2007 (Rigby et al., 2008; Dlugokencky et al., 2009). Amongst the varied surface sources of CH_4, the largest are natural wetlands, agriculture, livestock, biomass burning, waste and fossil fuel production; whereas the primary sink is the OH radical in the atmosphere (Kirschke et al., 2013; Saunois et al., 2020). Various hypotheses have been offered that attempt to attribute the behaviour in the global growth rate to a particular component or mechanism (Nisbet et al., 2016; Schaefer et al., 2016; Hausmann et al., 2016; McNorton et al., 2016b; Buchwitz et al., 2017a; Worden et al., 2017; Turner et al., 2017; Rigby et al., 2017) but currently there is no consensus within the community. Many of these studies have utilised satellite observations of atmospheric CH_4 and have shown the increasing capability of such measurements to characterise global and regional surface methane fluxes (Jacob et al., 2016).

This work presents the most recent update to the University of Leicester GOSAT Proxy XCH_4 Retrieval. This version (v9.0) now provides over a decade of global total column CH_4 observations, from April 2009 to December 2019. A full reprocessing of the entire time series has been performed to ensure consistency throughout the record and to ensure that results utilising the entire record are as robust as possible.

It is the intention of the authors that this study acts as a reference for everyone making use of the data and as such, we have attempted to provide as much practical detail as possible on the usage of the data.

Section 2 describes the GOSAT observations themselves and highlights any instrument anomalies or data gaps. Section 3 is broken down into several sub-sections detailing the usage of previous versions of this data by the scientific community. Section 4 gives an overview of the retrieval method and details the end-to-end data processing chain including statistics on throughput and data availability. Section 5 shows the validation of the data against the Total Carbon Column Observing Network, characterising not only the final Proxy XCH_4 data but also the individual components of the retrieval. Section 6 provides details of the global distribution of the data. Section 7 further characterises the data by performing model comparisons at global and regional scales. Finally we provide a summary and recommendations for future use in Section 8.

2 GOSAT TANSO-FTS Observations

GOSAT was launched in January 2009 by the Japanese Space Agency (JAXA), as the first satellite mission dedicated to making greenhouse gas observations (Kuze et al., 2009). GOSAT is nicknamed *"Ibuki"*, meaning *breath* in Japanese, highlighting that its mission involves monitoring the breathing of the planet, through measurement of the carbon cycle. In order to achieve this, GOSAT is equipped with a high-resolution Fourier Transform Spectrometer (TANSO-FTS - Thermal And Near infrared Sensor for carbon Observations – Fourier Transform Spectrometer). Shortwave infrared bands at 0.76 μm (O_2), 1.6 μm (CO_2

and CH_4) and 2.0 µm (CO_2) all provide near-surface sensitivity while a thermal infrared band between 5.5 and 14.3 µm provides mid-tropospheric sensitivity.

The objective for GOSAT was to provide routine measurements appropriate for regional and continental-scale flux estimates. Kuze et al. (2009) state a target relative accuracy of 2% for CH_4 over 3 month averages at 100-1000 km spatial scales. The
5 ESA GHG-CCI User Requirements Document (URD) specify goal (G), breakthrough (B) and threshold (T) requirements, with the goal requirements being the most stringent (Buchwitz et al., 2017a). For XCH_4 these values are 9, 17 and 34 ppb respectively for precision and 1, 5 and 10 ppb for relative accuracy. We discuss in Section 5 how we exceed these breakthrough requirements.

As an FTS acquisition is relatively slow ($\sim$4 seconds), the GOSAT sampling strategy is tailored to achieve this goal by
10 measuring with a relatively large footprint of 10.5 km, spaced apart approximately $\sim$263 km across-track and $\sim$283 km along-track. This means that while GOSAT does not "image" the surface, it does return to the same location every 3 days allowing a long time series of comparable measurements to be obtained. As well as nominally measuring over land in nadir mode, GOSAT is also capable of measuring over the ocean, which is normally too dark in the SWIR. This is achieved in the so-called "ocean sun-glint" observation mode, when the sun-satellite angle allows for a sufficiently reflected signal from the glint spot.
15 Discussion of the GOSAT measurement sampling strategy and its evolution over time can be found in Appendix E.

2.1 Instrument Anomalies and Data Gaps

Throughout its 10 years of operation, GOSAT has experienced a number of incidents resulting in instrument anomalies (Kuze et al., 2016). These incidents include:

- May 2014 - a solar paddle incident resulting in a temporary instrument shutdown.

20 - January 2015 - a switch to the secondary pointing mechanism due to degradation of the primary system.

- August 2015 - a cryocooler shutdown and restart.

- May 2018 - a CDMS (Command and Data Management System) incident resulting in GOSAT being inactive for 2 weeks.

- November 2018 - rotation anomaly of the second solar paddle.

25 The temporary reduction in observations related to these incidents is discussed in Section 4.3 and reflected in Figure 4.

3 Studies Utilising Proxy XCH_4 Data

The University of Leicester GOSAT Proxy XCH_4 data is produced operationally for the ESA Greenhouse Gas Climate Change Initiative (Buchwitz et al., 2017b) and the Copernicus Climate Change Service (C3S) (Buchwitz et al., 2018) as well as routinely for the UK National Centre for Earth Observation. This work details Version 9.0 of the University of Leicester

5

GOSAT Proxy XCH$_4$ data but previous versions over the past decade have been used for a wide variety of scientific studies. This section details some of these past studies in order to highlight the potential applications for this data.

3.1 Validation of data

Firstly, before any conclusions can be drawn from analysis of the data, the data itself must be validated to ensure its robustness and reliability. Previous versions of the data have been extensively validated against the TCCON network (Total Carbon Column Observing Network) as part of the ESA Climate Change Initiative (Parker et al., 2011; Dils et al., 2014; Buchwitz et al., 2017a), including extensive validation of the model XCO$_2$ used in the generation of the data (Parker et al., 2015). We have also performed validation of the data against aircraft profile observations over the Amazon (Webb et al., 2016), one of the most important and challenging regions for the retrieval.

3.2 Comparison to other satellite observations

Although GOSAT was the first satellite mission dedicated to measuring GHGs, successful CH$_4$ retrievals were performed previously from SCIAMACHY and continue to be performed from new missions such as TROPOMI onboard Sentinel 5-Precursor and the recently launched GOSAT-2. Furthermore, many thermal infrared missions are capable of measuring CH$_4$ (IASI, AIRS, TES, CrIS), albeit with sensitivity to the mid-troposphere and little sensitivity to the surface. Nevertheless, it is important that these different observations are consistent and their capabilities well-understood if we wish to perform long-term analysis. The ESA Greenhouse Gas Climate Change Initiative (ESA GHG-CCI) (Buchwitz et al., 2017a) made substantial efforts to characterise and validate these different observations (Dils et al., 2014). The ensemble median algorithm (EMMA) (Reuter et al., 2020) homogenises the SCIAMACHY and GOSAT datasets produced via the ESA GHG-CCI project and is intended to be a long time series dataset for climate applications.

Studies such as Cressot et al. (2014) and Alexe et al. (2015) have investigated the consistency between flux inversions utilising SCIAMACHY, GOSAT (and IASI) CH$_4$ observations and generally found good consistency in derived emissions. Worden et al. (2015) combined the surface sensitivity of GOSAT with the mid-tropospheric sensitivity of the NASA TES instrument to better estimate the lower tropospheric methane (and hence surface) emissions while Siddans et al. (2017) have compared their IASI CH$_4$ product to GOSAT observations, finding good consistency between the two.

3.3 Investigation of the global growth rate

Perhaps the most important scientific question related to atmospheric CH$_4$ concentrations is understanding the observed long-term behaviour. The cause of the so-called "hiatus" or plateau in atmospheric CH$_4$ between 2000 and 2007 remains unresolved with various studies speculating on the reason. Although the GOSAT record unfortunately only began in 2009, after the end of the plateau period, it can still help to characterise behaviour and understand the processes that may have contributed to the stalling. GOSAT data have been successfully used to infer long-term global fluxes. As well as contributing to the Global Methane Budget assessments (Saunois et al., 2016, 2020), GOSAT data have been used to assess the role of regional wet-

land emissions ~~(McNorton et al., 2016b)~~ (McNorton et al., 2016b; Maasakkers et al., 2019) and the role of OH variability as a potential cause for the stalling in growth rate (McNorton et al., 2016a; Maasakkers et al., 2019).

3.4 Regional emissions

GOSAT data have been successfully utilised in regional-scale studies to determine CH_4 fluxes over many different regions. These types of studies are of particular interest as they can help inform policy-related discussions on validation and verification of regional or country-scale emission targets, such as those relevant to the Paris Agreement (Bergamaschi et al., 2018a). Fraser et al. (2013) performed regional flux inversions and found large changes over Temperate Eurasia and Tropical Asia, with the satellite observations providing a significant error reduction over only using surface data. Wecht et al. (2014) performed continental-scale inversions over North America and produced estimates of Californian CH_4 emissions and found consistent emission estimates over the Los Angeles Basin between the satellite inversion and that from a dedicated aircraft campaign. Turner et al. (2015) extended this work to the entire US and inferred a US anthropogenic CH_4 source over 50% larger than that from EDGAR and EPA bottom-up inventories. Satellite inversion results from Alexe et al. (2015) showed a ~~redistributon~~ redistribution of CH_4 emissions in the US from the north-east to south-central. These results are consistent with recent independent studies that suggest that bottom-up estimates of North American fossil fuel emissions (particularly related to natural gas and petroleum production facilities) are ~~systemtically~~ systematically underestimated. Ganesan et al. (2017) used GOSAT data to infer India's CH_4 emissions between 2010-2015 and found average emissions of 22.0 Tg yr^{-1} to be consistent with the emissions reported by India to the UNFCCC with no significant trend over time. Sheng et al. (2018) performed a similar study over the US, Canada and Mexico and found that US emissions increased by 2.5% over the 7-year study period and attributed this to contributions from the oil and gas industry and livestock. In Feng et al. (2017) the individual XCO_2 and XCH_4 components from the Proxy retrieval are used to infer regional CO_2 and CH_4 fluxes simultaneously. Finally, Lunt et al. (2019) inferred CH_4 emissions over tropical Africa and found a linear increase of between 1.5 and 2.1 Tg yr^{-1} for 2010-2016, attributing much of this to short-term increase in emissions over the Sudd wetland area in South Sudan.

4 UoL Proxy XCH$_4$ Retrieval

The University of Leicester Full-Physics retrieval algorithm (UoL-FP) is based on the original NASA Orbiting Carbon Observatory (OCO) "Full-Physics" retrieval algorithm (Connor et al., 2008; Boesch et al., 2011; O'Dell et al., 2012) which was designed to simultaneously fit the short-wave infrared radiances in the 0.76 μm O_2-A band and the 1.6 μm and 2 μm CO_2 bands. This algorithm has been adapted for use on GOSAT observations and modified to perform a variety of different retrievals, including the Proxy method described here. The radiative transfer calculations are accelerated using the Low-Stream Interpolation approach (O'Dell, 2010).

The concept behind the Proxy XCH_4 retrieval approach (Frankenberg et al., 2006) is that the majority of atmospheric scattering and instrument effects will be similar for CH_4 and CO_2 mole fraction retrievals performed in a common absorption band (around 1.6 μm, where both CO_2 and CH_4 have absorption features). By taking the ratio of the retrieved XCH_4/XCO_2,

the CO_2 acts as a "proxy" for the modifications to the light path induced by scattering (Butz et al., 2010) and cancels out those in the CH_4 retrieval. This means that moderate aerosol scattering does not adversely impact upon the retrieval, resulting in a higher number of high-quality XCH_4 observations compared to the full-physics approaches where much stricter post-filtering are often required. This is especially useful over the tropics, where moderate aerosol or cirrus effects can limit the coverage of full-physics methods but affect the proxy approach far less severely.

In order to convert the retrieved XCH_4/XCO_2 ratio into a final XCH_4 quantity, a model-based estimate of XCO_2 is used, according to the equation:

$$\mathrm{XCH}_{4(\text{proxy})} = \frac{\mathrm{XCH}_4}{\mathrm{XCO}_2} \times \mathrm{XCO}_{2(\text{model})} \tag{1}$$

where the relative variability of CO_2 in the atmosphere is known to be much lower than that of CH_4. This leads to the primary disadvantage of this method, i.e. that the model-based estimates of XCO_2 may introduce biases in the retrieved CH_4. In an attempt to minimise such biases, CO_2 dry-air mole fractions $XCO_{2(\text{model})}$ used in Eq. (1) in the UoL proxy retrieval scheme are obtained by taking the median of the estimates produced by three atmospheric chemistry transport models which have assimilated surface in-situ data: GEOS-Chem (Feng et al., 2011), NOAA CarbonTracker (Peters et al., 2007), and CAMS (Chevallier et al., 2010).

The advantage of the Proxy retrieval approach compared to the "Full-Physics" retrieval as typically used for CO_2 (Boesch et al., 2011; Cogan et al., 2012), is that Proxy retrievals are less sensitive to instrumental effects, and require less-strict quality filtering (Schepers et al., 2012; Parker et al., 2015), thereby ensuring a better coverage of regions (especially in the tropics), where Full-Physics retrievals are particularly challenging.

4.1 Retrieval Inputs and A Priori Generation

In order to prepare all of the necessary inputs to the retrieval, we use the Leicester Retrieval Preparation Toolset (LRPT) software. The latest version of the GOSAT Level 1B files (version 210.210) are acquired directly from the NIES GDAS Data Server and are processed with the LRPT to extract the measured radiances along with all required sounding-specific ancillary information such as the measurement time, location and geometry. These measured radiances have the recommended radiometric calibration and degradation corrections applied as per Yoshida et al. (2013) with an estimate of the spectral noise derived from the standard deviation of the out-of-band signal. We then format the spectral data for input into the UoL-FP retrieval algorithm and generate a list containing all of the ancillary data necessary to create the retrieval a priori information.

Sounding-specific a priori information are generated for all individual soundings present in the sounding-selector list above. Atmospheric temperature and water vapour profiles are taken from ECMWF ERA-Interim up to August 2019 and ERA-5 thereafter. CO_2 profile information is taken from the 16r1 CAMS atmospheric inversion (Chevallier, 2019) and incremented by the NOAA estimated global growth rate for recent years. CH_4 profiles are taken from a combination of the MACC-II CH_4 inversion (v10-S1NOAA - https://apps.ecmwf.int/datasets/data/macc-ghg-inversions/) for the troposphere and from a dedicated
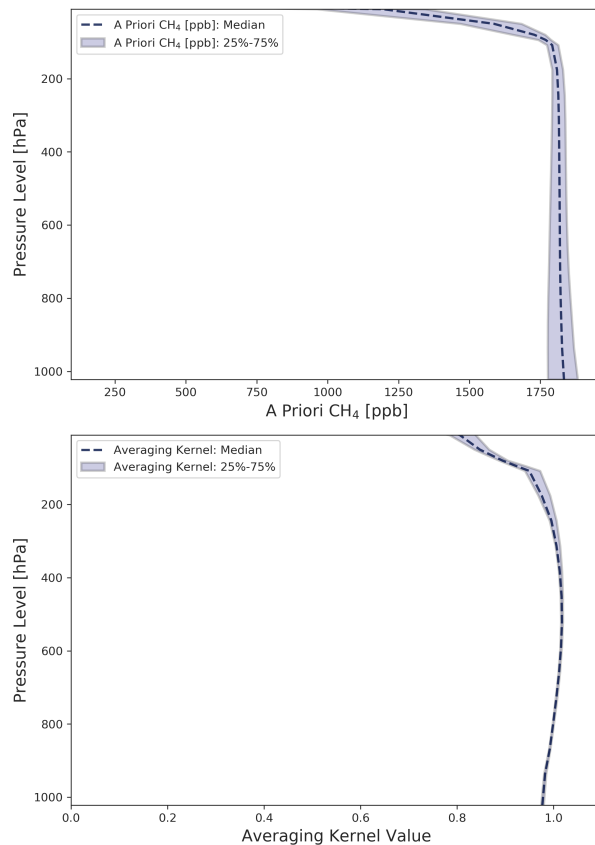
Figure 1. The average CH$_4$ a priori profile used in the retrievals along with the 25-75% variation (top). The average normalised column averaging kernel produced by the retrieval along with the 25-75% variation, highlighting the strong sensitivity of the retrieval to the surface (bottom).
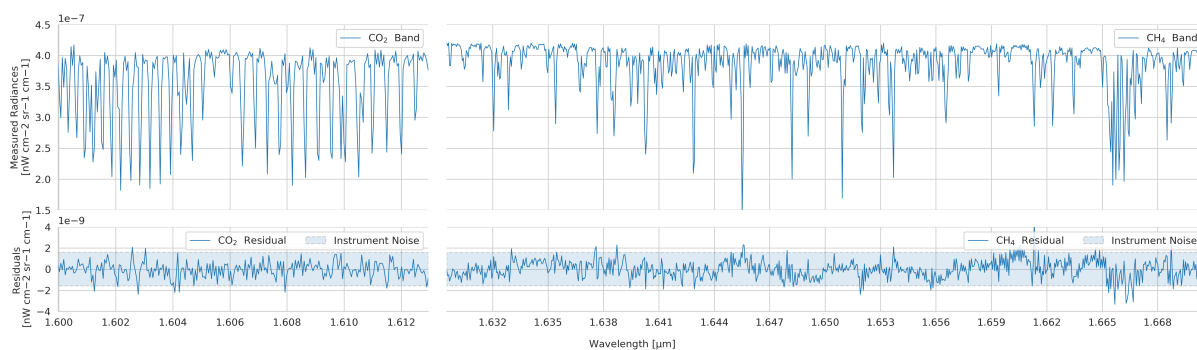

Figure 2. Spectra showing the GOSAT radiances for the CO$_2$ and CH$_4$ bands and the resulting residuals (measured - simulated spectral differences). The data shown are the median values for the 25,274 land retrievals that pass the quality filtering for an example month, August 2016.

TOMCAT stratospheric chemistry model simulation (Chipperfield, 1999) for the stratospheric component. This ensures that the CH_4 a priori profiles are sufficiently vertically resolved and capture the sharp decrease in concentration around the tropopause (Figure 1 (top)). As the MACC-II data is only available until 2012, the data after this period is repeated each year.
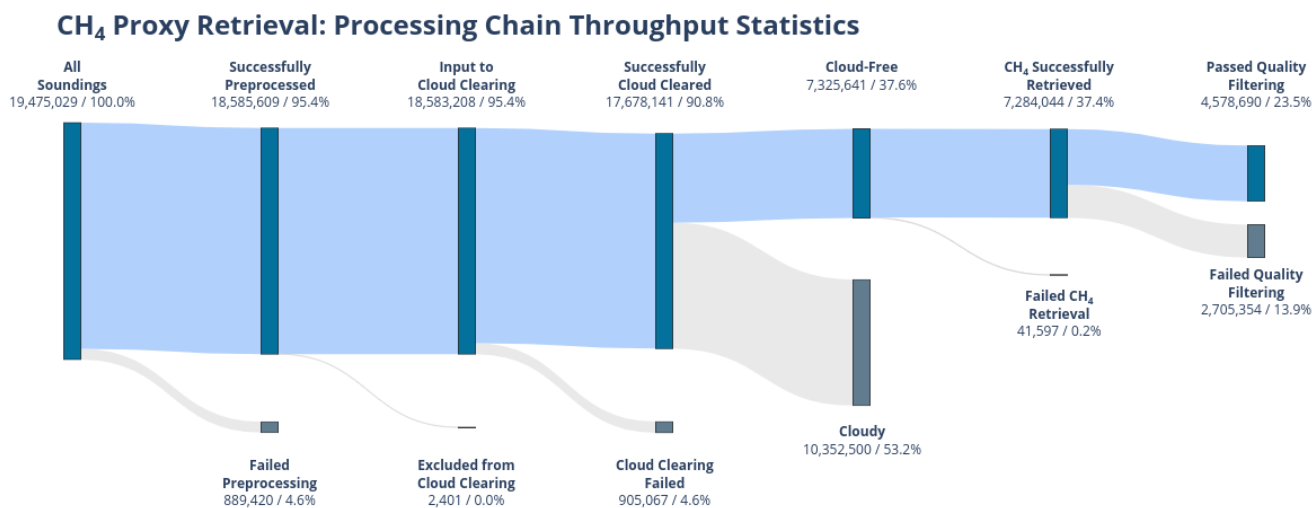
CH_4 Proxy Retrieval: Processing Chain Throughput Statistics

Figure 3. Sankey diagram detailing the retrieval throughput at each step of the processing chain for the GOSAT Proxy XCH_4 retrieval. As well as the absolute number of soundings, the percentage relative to the initial total is also given.

All of the atmospheric profiles are then interpolated to a sounding-specific retrieval grid. For each sounding a 20-level pressure-based retrieval grid is generated that ranges from the top of the atmosphere (0.1 hPa) to 20 hPa beneath the surface pressure as estimated by ERA-Interim. This 20 hPa buffer allows the surface pressure to be adjusted during the initial cloud-screening process without leading to unphysical extrapolation of the a priori profiles.

In addition to atmospheric a priori information, we also generate sounding-specific a priori information for the spectral dispersion and surface albedo directly from the GOSAT spectra.

The retrieval algorithm also requires the input of spectroscopic parameters for the species being simulated. We use v4.2.0 of the OCO line lists for CO_2, H_2O and O_2, and take CH_4 parameters from the TCCON line lists (Toon, 2015).

4.2 Cloud-Screening

Prior to the XCH_4 and XCO_2 retrievals, cloudy GOSAT soundings are identified and excluded by using the UoL-FP retrieval algorithm to obtain the apparent surface pressure from O_2 A-band spectra and comparing it to the surface pressure provided by the ECMWF reanalysis (Dee et al., 2011). If the absolute difference between the retrieved and the ECMWF surface pressure is larger than 30 hPa, a sounding is flagged as cloudy and excluded from further processing. The reason why a loose threshold is used for the surface pressure difference is that this procedure only aims to identify and remove soundings which are significantly

cloudy. Partially cloudy scenes, or scenes where optically thin clouds are present, are processed by the retrieval algorithm, and are dealt with through a post-retrieval quality filtering scheme described later in this section.

4.3   XCH$_4$ and XCO$_2$ Retrievals

For soundings that pass the cloud screening procedure described above, retrievals with the UoL-FP algorithm for CO$_2$ and
5 CH$_4$ mole fraction profiles are carried out separately. The state vector for these retrievals consists of 20-level profiles for CH$_4$ and CO$_2$ mole fractions along with profile scaling factors for H$_2$O mole fraction and temperature with parameters for surface albedo and spectral dispersion also included allowing us to explicitly fit the wavelength for each spectra independently.

A post-retrieval quality filtering is then carried out, by selecting the retrievals that meet the following criteria: (1) goodness-of-fit (χ^2) parameter between 0.4 and 1.9 for both CH$_4$ and CO$_2$; (2) a posteriori error smaller than 20 ppb for CH$_4$ and 3 ppm
10 for CO$_2$; (3) retrieved XCH$_4$ larger than 1650 ppb and XCO$_2$ larger than 350 ppm; and (4) latitude north of 60°S (to exclude Antarctica).

Figure 2 shows an example of the spectral fits for one month of data (August 2016) for all 25,274 successful, quality-filtered data measured over land. The top panels show the averaged measured radiances in the 1.6 μm CO$_2$ (left) and 1.65 μm CH$_4$ (right) retrieval windows, with the bottom panels showing the residual differences to the final simulated spectra. The estimated
15 instrument noise is indicated by the shaded area and the residuals are found to be within the noise.

The retrieved XCH$_4$ and XCO$_2$ satisfying the aforementioned quality criteria are then used in Eq. (1), together with the ensemble median model XCO$_2$ described earlier in this section. Prior to the calculation of XCO$_2$ to be used in Eq. (1), model CO$_2$ profiles are convolved with scene-dependent instrument averaging kernels computed as part of the CO$_2$ retrieval.

Before the final production of the data files, an offset is subtracted from the retrieved XCH$_4$ to remove a residual mean bias
20 to TCCON (see Section 5). Currently, a single offset value of 9.06 ppb is used. This offset is applied to all analysis presented here and is built-in to the final delivered data.

A summary of the throughput of the whole processing chain described in this section is shown in Fig. 3. This shows that in total, between April 2009 and December 2019 we have 19.5 million individual GOSAT soundings which are ingested into the LRPT software. Of these, 95.4% are successfully preprocessed, with the 4.6% that fail largely due to incomplete or invalid L1B
25 data. A very small number of successfully preprocessed soundings < 0.1% are unable to be processed further as we are unable to estimate a noise for those spectra. Of the 18.6 million soundings that continue and are attempted for cloud-clearing, 17.7 million are able to be successfully cloud-cleared. Of these, just over 7 million soundings are found to be cloud free, with over 10 million determined to be cloudy. A successful CH$_4$ retrieval is performed on the majority of these cloud-free soundings, with just 41,597 failing the retrieval. Of the 7.3 million successful CH$_4$ retrievals, 2.7 million are rejected by our final quality
30 filtering. It should be noted that currently we exclude all retrievals below 60°S (i.e. Antarctica) due to low signal-to-noise and difficulty in distinguishing low cloud from the ~~snpw-covered~~ snow-covered surface. This alone accounts for over 1 million of the 2.7 million rejected retrievals. Finally, we are left with almost 4.6 million successful and quality-controlled XCH$_4$ retrievals (23.5% of the total measurements performed).
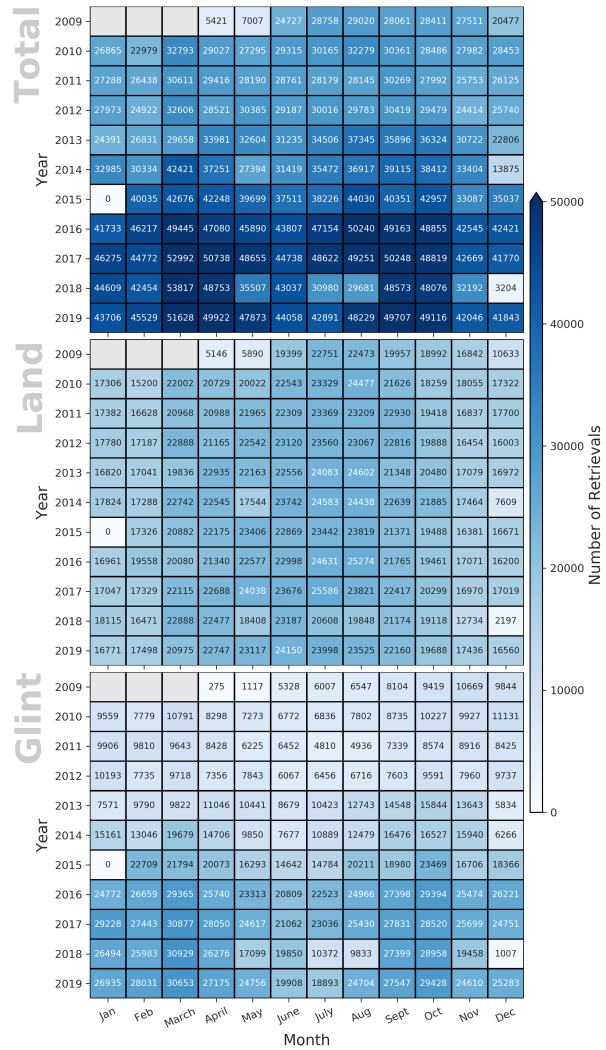
Figure 4. The number of GOSAT soundings per month in the final Proxy XCH$_4$ dataset, starting in April 2009 and ending in December 2019. Counts are provided for the global total but also for land and glint observation modes separately.

Total

Year	Jan	Feb	March	April	May	June	July	Aug	Sept	Oct	Nov	Dec
2009				5421	7007	24727	28758	29020	28061	28411	27511	20477
2010	26865	22979	32793	29027	27295	29315	30165	32279	30361	28486	27982	28453
2011	27288	26438	30611	29416	28190	28761	28179	28145	30269	27992	25753	26125
2012	27973	24922	32606	28521	30385	29187	30016	29783	30419	29479	24414	25740
2013	24391	26831	29658	33981	32604	31235	34506	37345	35896	36324	30722	22806
2014	32985	30334	42421	37251	27394	31419	35472	36917	39115	38412	33404	13875
2015	0	40035	42676	42248	39699	37511	38226	44030	40351	42957	33087	35037
2016	41733	46217	49445	47080	45890	43807	47154	50240	49163	48855	42545	42421
2017	46275	44772	52992	50738	48655	44738	48622	49251	50248	48819	42669	41770
2018	44609	42454	53817	48753	35507	43037	30980	29681	48573	48076	32192	3204
2019	43706	45529	51628	49922	47873	44058	42891	48229	49707	49116	42046	41843

Land

Year	Jan	Feb	March	April	May	June	July	Aug	Sept	Oct	Nov	Dec
2009				5146	5890	19399	22751	22473	19957	18992	16842	10633
2010	17306	15200	22002	20729	20022	22543	23329	24477	21626	18259	18055	17322
2011	17382	16628	20968	20988	21965	22309	23369	23209	22930	19418	16837	17700
2012	17780	17187	22888	21165	22542	23120	23560	23067	22816	19888	16454	16003
2013	16820	17041	19836	22935	22163	22556	24083	24602	21348	20480	17079	16972
2014	17824	17288	22742	22545	17544	23742	24583	24438	22639	21885	17464	7609
2015	0	17326	20882	22175	23406	22869	23442	23819	21371	19488	16381	16671
2016	16961	19558	20080	21340	22577	22998	24631	25274	21765	19461	17071	16200
2017	17047	17329	22115	22688	24038	23676	25586	23821	22417	20299	16970	17019
2018	18115	16471	22888	22477	18408	23187	20608	19848	21174	19118	12734	2197
2019	16771	17498	20975	22747	23117	24150	23998	23525	22160	19688	17436	16560

Glint

Year	Jan	Feb	March	April	May	June	July	Aug	Sept	Oct	Nov	Dec
2009				275	1117	5328	6007	6547	8104	9419	10669	9844
2010	9559	7779	10791	8298	7273	6772	6836	7802	8735	10227	9927	11131
2011	9906	9810	9643	8428	6225	6452	4810	4936	7339	8574	8916	8425
2012	10193	7735	9718	7356	7843	6067	6456	6716	7603	9591	7960	9737
2013	7571	9790	9822	11046	10441	8679	10423	12743	14548	15844	13643	5834
2014	15161	13046	19679	14706	9850	7677	10889	12479	16476	16527	15940	6266
2015	0	22709	21794	20073	16293	14642	14784	20211	18980	23469	16706	18366
2016	24772	26659	29365	25740	23313	20809	22523	24966	27398	29394	25474	26221
2017	29228	27443	30877	28050	24617	21062	23036	25430	27831	28520	25699	24751
2018	26494	25983	30929	26276	17099	19850	10372	9833	27399	28958	19458	1007
2019	26935	28031	30653	27175	24756	19908	18893	24704	27547	29428	24610	25283

Figure 4 shows the number of successful retrievals broken down by month and also split into land and glint observation modes. This figure is particularly useful as it highlights any systematic differences in data density over time (e.g. from changes in the GOSAT sampling strategy) and also highlights abrupt data gaps (e.g. from instrument anomalies). In particular, it shows that the increase in monthly data from 2014/2015 onwards is largely a result of an increase in the number of glint observations which is a direct result of the instrument sampling changes that increased the valid glint range. This does highlight that some care should be taken when using the data for some applications as there cannot be assumed consistent temporal/spatial data coverage over the whole data record. Large data gaps, such as in January 2015 and December 2018 are also highlighted and indicate where care may need to be taken when analysing over these periods.
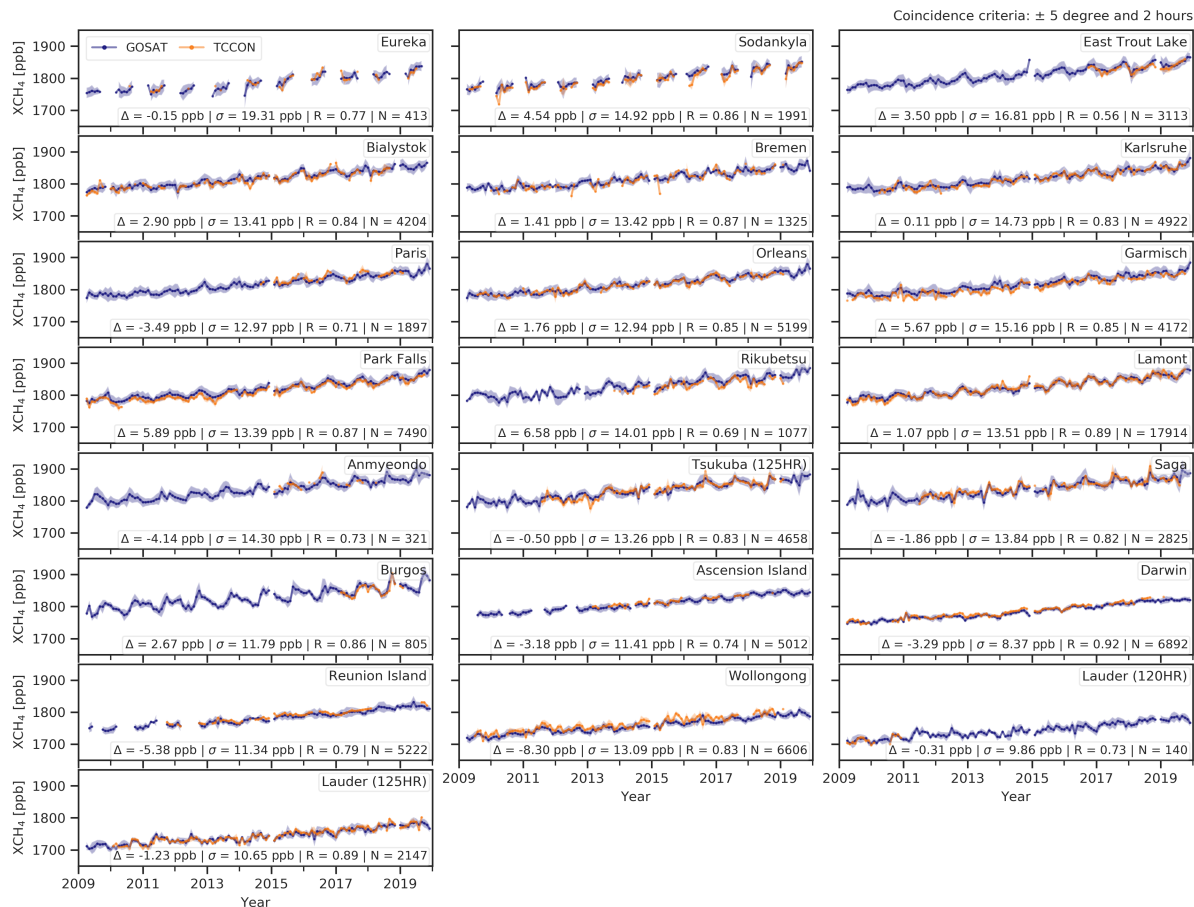
Figure 5. Time series plots for each TCCON site comparing GOSAT Proxy XCH$_4$ data to the matching co-located TCCON measurements. Statistics for each site are included, showing the average GOSAT-TCCON difference, the GOSAT-TCCON standard deviation, the correlation coefficients and the number of co-located GOSAT-TCCON measurements.

5 Validation Against TCCON

Evaluation against the Total Carbon Column Observing Network (TCCON) is the primary mechanism by which satellite-based measurements of XCO$_2$ and XCH$_4$ are validated.

The TCCON network consists of ground-based high-resolution Fourier transform spectrometers, performing direct measurements of solar spectra in the near-infrared. There are currently 27 operational sites located across North America, Europe, Asia and Oceania, including several islands in the southern hemisphere and other remote areas. TCCON sites have become operational at different times (see Table A1) and hence the data record length varies between sites, with Burgos (~~Phillipines~~Philippines) (Velazco et al., 2017) and Nicosia (Cyprus) the most recent to come online in 2017 and 2019 respectively. Also note that the Lauder site (Pollard et al., 2017) has multiple instruments and we have kept these records separate.

13
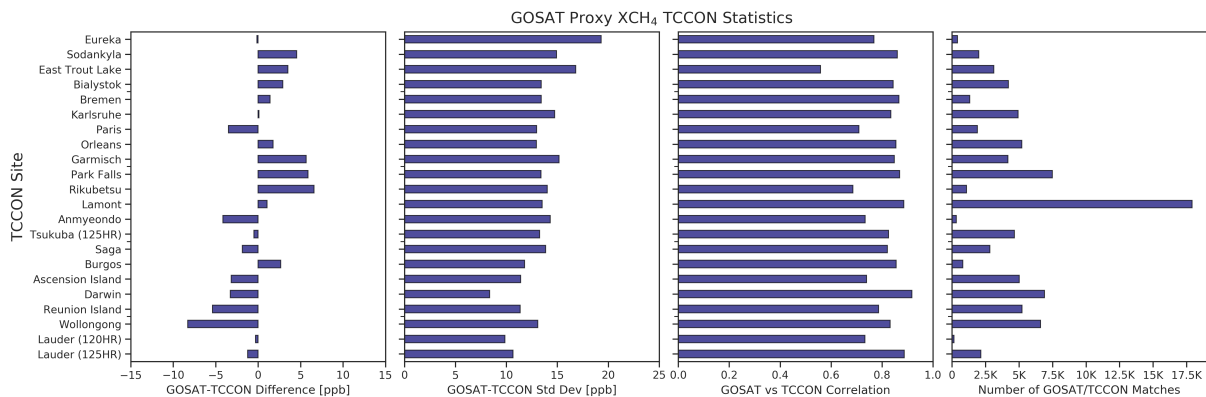
Figure 6. Summary of the statistics from Figure 5 comparing the GOSAT Proxy XCH$_4$ data to the TCCON measurements for each TCCON site. Panels show the GOSAT-TCCON difference, the GOSAT-TCCON standard deviation, the correlation coefficients between the GOSAT and TCCON data and finally the number of co-located GOSAT-TCCON measurements.

TCCON has been used extensively to validate satellite observations of XCH$_4$ from SCIAMACHY (De Mazière et al., 2004; Dils et al., 2006), GOSAT (Dils et al., 2014; Parker et al., 2011; Yoshida et al., 2013; Parker et al., 2015; Inoue et al., 2016) and TROPOMI (Hu et al., 2018; Schneising et al., 2019; Lambert et al., 2019) and allows these measurements to be bias-corrected where necessary. TCCON itself is tied to the World Meteorological Organization (WMO) standard through comparison against

5 integrated aircraft measurements (Wunch et al., 2010, 2011).

This work uses the latest available TCCON data, GGG2014. Detailed dataset citations are available for each site in Table A1.

For comparison between TCCON and GOSAT, all GOSAT soundings within $\pm 5°$ of a TCCON site are taken. For these soundings, the average of the TCCON data within ± 2 hours of the GOSAT overpass time is calculated, resulting in GOSAT-

10 TCCON pairs when there is TCCON data available. It is these matched GOSAT-TCCON pairs that are then subsequently analysed. In total we use 22 of these sites within our analysis (see Table A1), omitting some sites with insufficient data coverage or high-altitude sites where the total column may not be well-represented or co-located well to the satellite observations. Figure 5 shows the time series of the GOSAT (blue) and TCCON (orange) data between 2009 and 2019 for each individual site. Also provided are the mean GOSAT-TCCON difference (Δ), the standard deviation of the GOSAT-TCCON difference

15 (σ), the correlation coefficient (R) and the total number of GOSAT-TCCON pairs (N). These statistics are also summarised in Figure 6 which show that generally the GOSAT-TCCON difference is small (< 5 ppb), the standard deviation (which can be considered to be the single measurement precision of the GOSAT data) is typically between 10-15 ppb, the correlation coefficient is generally high (0.7-0.9) and there are many co-located GOSAT-TCCON measurements with the distribution changing considerably between TCCON sites. Another important validation metric is the relative accuracy, or inter-station

20 bias. This metric is an indication of any spatio-temporal variability of the bias and is defined in Dils et al. (2014) as the standard deviation of the individual site biases. We obtain a value of 3.89 ppb for this metric, again smaller than the estimated

14
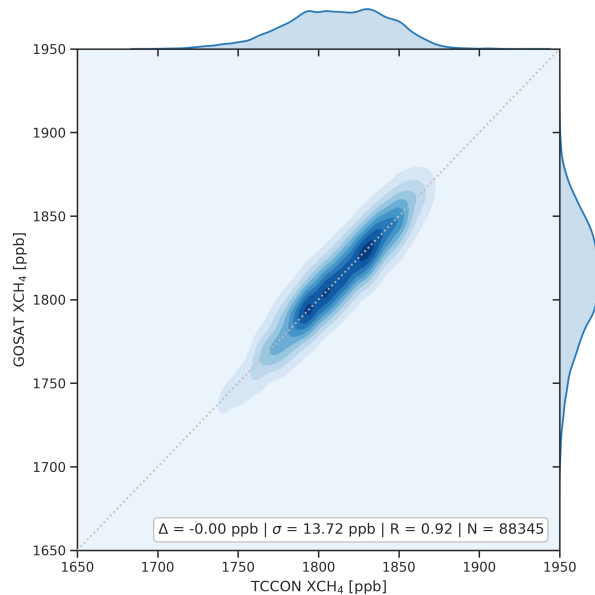
Figure 7. Correlation between the 88,345 matching TCCON XCH_4 data and co-located GOSAT Proxy XCH_4 measurements across all TCCON sites. The data is presented as a 2-dimension kernel density estimation (KDE) plot. The distribution sites along the one-to-one line (grey dashed) with a standard deviation (i.e. single-sounding precision) of 13.68 ppb and a correlation coefficient (r) of 0.91. An overall bias to TCCON of 9.06 ppb is removed from the GOSAT data, resulting in an average bias of 0 ppb by design. The individual KDE plots are shown along the upper and right margins.

TCCON accuracy of ± 4 ppb. This meets the "breakthrough" user requirement for the systematic error of 5 ppb as defined by Buchwitz et al. (2017a).

In total across all TCCON sites we find 88,345 matching GOSAT-TCCON data pairs. The correlation between the GOSAT and TCCON data is shown in Figure 7, presented as a 2-D kernel density estimation (KDE) plot, along with the corresponding

5 marginal 1-D KDE plots on the X and Y axes. An overall difference of 9.06 ppb is removed from the GOSAT data so that, by design, the absolute average difference to TCCON is 0 ppb. The overall standard deviation or single measurement precision is found to be 13.72 ppb with a correlation coefficient of 0.92. The single measurement precision of 13.72 ppb ~~surpasses the "breakthrough " random error user~~ comfortably exceeds the precision breakthrough requirement of 17 ppb ~~as specified by Buchwitz et al. (2017a)~~(Buchwitz et al., 2017a) indicating that it "would result in a significant improvement for the targeted

10 application". Although the data contributing to this plot are from a wide variety of TCCON sites in different locations and at different latitudes, the distribution appears consistent and is tightly aligned to the one-to-one (dashed) line. However, there are signs of ~~potentially a~~ a potential hemispheric or latitudinal bias in the data against TCCON, although this is not apparent at all sites; for example Karlsruhe, Lamont, Tsukuba and Lauder all have negligible biases but span a large latitude range. It should also be noted that the uncertainty on the TCCON XCH_4 is approximately 4 ppb and for the majority of sites the

15 GOSAT-TCCON difference is within this uncertainty so care must be taken to not over-interpret any signals at this scale.

15
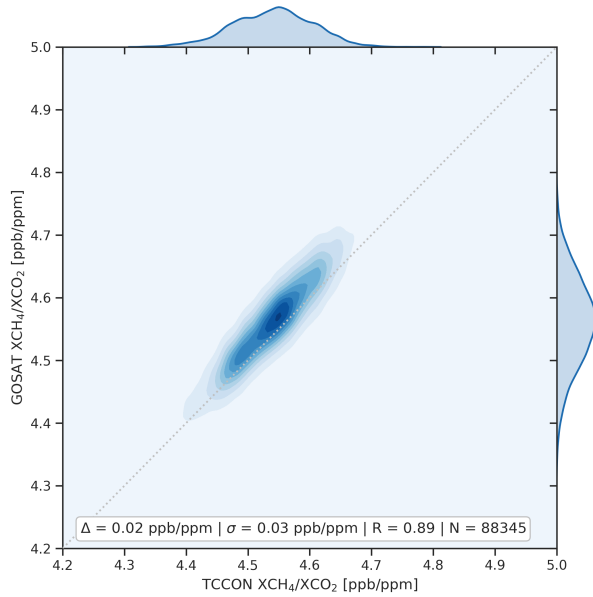
Figure 8. Correlation between the 88,345 matching TCCON XCH_4/XCO_2 ratios and co-located GOSAT XCH/XCO_2 ratios retrieved as a raw fundamental part of the Proxy XCH_4 retrieval (Equation 1). The data is presented as a 2-dimension kernel density estimation (KDE) plot. The distribution sites along the one-to-one line (grey dashed) with a standard deviation of 0.03 ppb/ppm and a correlation coefficient (r) of 0.89. An overall bias to TCCON of 0.02 ppb/ppm is present in this raw data. The individual KDE plots are shown along the upper and right margins.

5.1 XCH_4/XCO_2 Ratio Validation

In addition to validation of our final XCH_4 Proxy dataset, TCCON data allow us the opportunity to validate the different components in Equation 1, namely the XCH_4/XCO_2 ratio and the model-derived XCO_2.

Figure 8 shows the correlation between the retrieved GOSAT XCH_4/XCO_2 ratio (ppb/ppm) (with no bias correction applied)
5 and the corresponding ratio calculated from TCCON. There is an excellent correlation coefficient of 0.89 across the 88,345 matching data points with a standard deviation of just 0.03 ppb/ppm. An average offset between the two datasets of 0.02 ppb/ppm exists and is of a very similar magnitude to the global offset that is removed from the final data of 9.06 ppb. To be clear, the final bias correction which we apply to the Proxy XCH_4 is almost entirely attributed to this bias that we identify here in the XCH_4/XCO_2 ratio. It should also be noted here that the TCCON data itself has a bias correction applied to the
10 XCO_2 and XCH_4 data. This airmass-independent correction factor derived from airborne calibrations is 1/0.9898 for XCO_2 and 1/0.9765 for XCH_4 (Wunch et al. (2010) - Table 5). It is considered that this correction is mainly a result of deficiencies in the spectroscopy, which likely apply to the GOSAT retrievals as well and might go some way to explaining this small difference between TCCON and GOSAT.

5.2 Validation of XCO$_2$ Model

To validate the XCO$_2$ model data used in the generation of the final Proxy data, we evaluate the model median XCO$_2$ mixing ratios against TCCON but also evaluate the three individual models, sampled at the time and location of the GOSAT soundings, with the GOSAT sounding-specific averaging kernel applied. These XCO$_2$ models are all independent of TCCON data but do assimilate NOAA surface site measurements, some of which are nearby to TCCON sites. Figure 9 shows the correlation between TCCON and the Model Median XCO$_2$ (top left), GEOS-Chem XCO$_2$ (top right), CAMS XCO$_2$ (bottom left) and CarbonTracker XCO$_2$ (bottom right). In all four cases there is an excellent agreement between TCCON and the model data with correlation coefficients all at 0.99, with average differences ranging from -0.07 ppm to 0.17 ppm and standard deviations between 1.02 ppm to 1.17 ppm. Although the values are all very similar, the model with the smallest difference (GEOS-Chem) has the largest standard deviation and conversely the model with the largest difference (CAMS) has the smallest standard deviation. Overall the Model Median performs marginally better than any of the individual models with a standard deviation of 1.02 ppm but retaining a very small difference (0.08 ppm). Parker et al. (2015) provides a detailed assessment of the contribution to the overall uncertainty on the Proxy XCH$_4$ related to the model XCO$_2$.
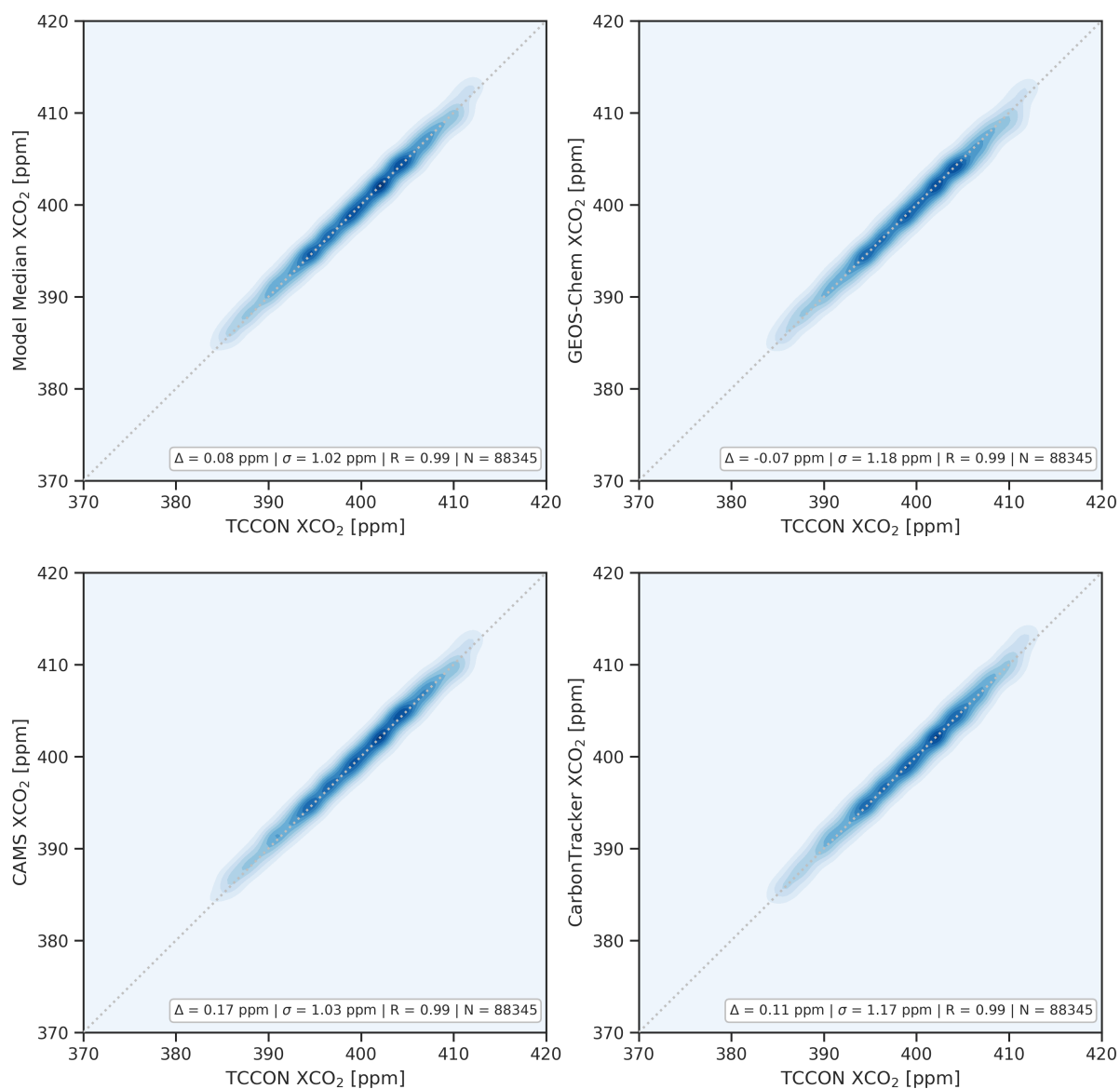
Figure 9. Correlation of the individual XCO$_2$ models (GEOS-Chem, MACC and Carbon-Tracker) used in the generation of the GOSAT Proxy XCH$_4$ data against matching co-located TCCON XCO$_2$ measurements. The first panel shows the median model value which is the quantity directly used in Equation 1 to generate the final Proxy XCH$_4$ quantities. The data is presented as a 2-dimension kernel density estimation (KDE) plot with the one-to-one line shown as the grey dashed line. Also included are the statistics (difference, standard deviation, correlation coefficient and number of matching measurements) comparing each model to the TCCON XCO$_2$.
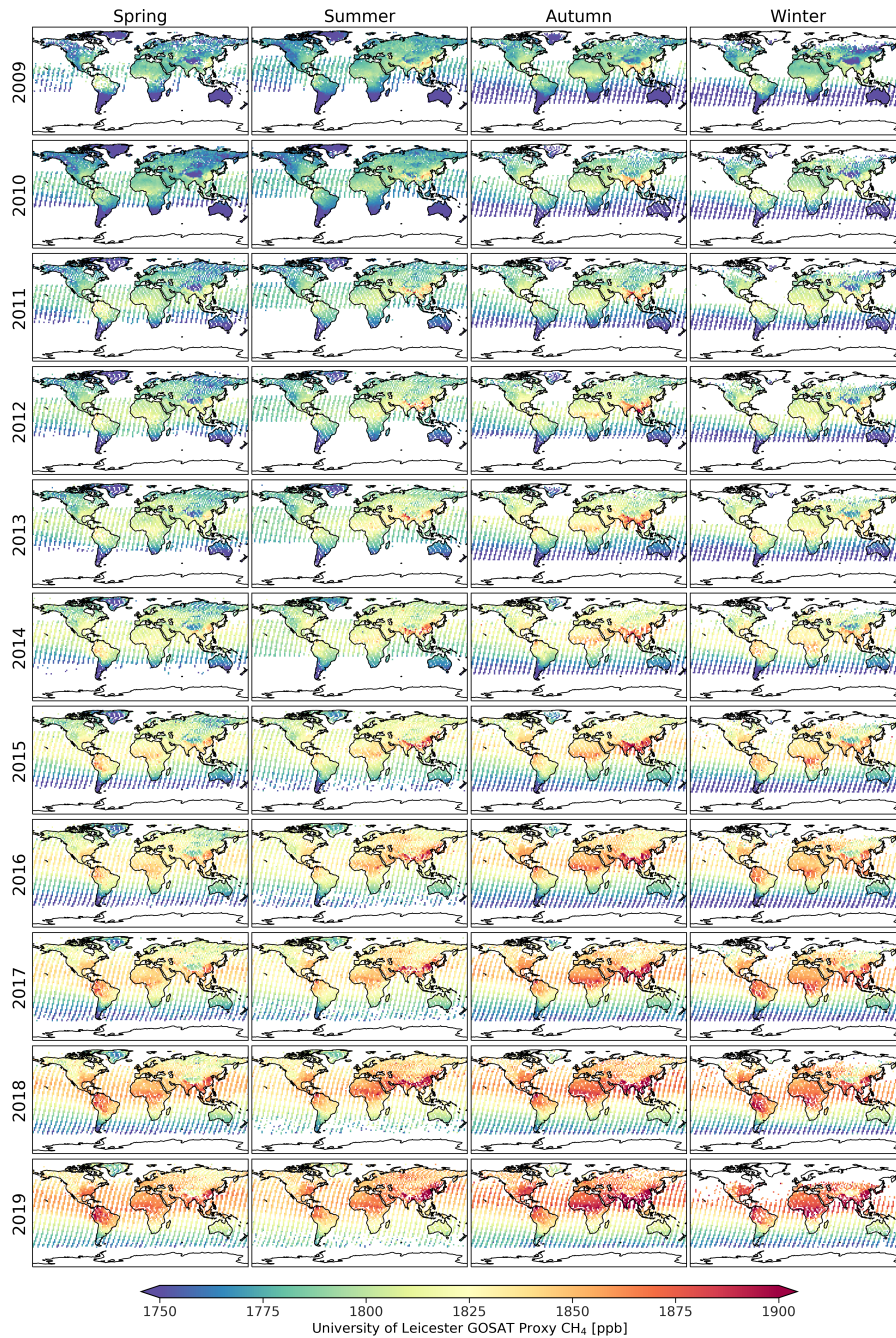
Figure 10. Global maps showing the GOSAT Proxy XCH$_4$ data from April 2009 to December 2019 separated into seasons - Spring (MAM), Summer (JJA), Autumn (SON) and Winter (DJF).
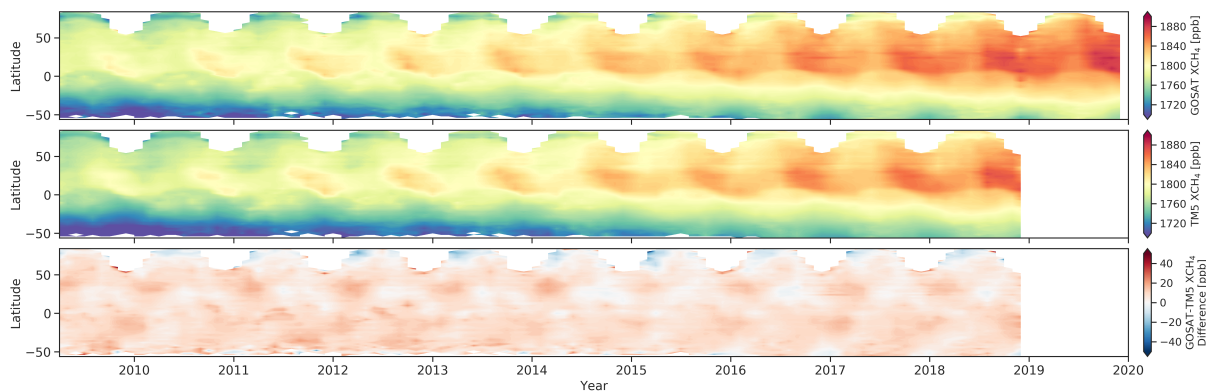
Figure 11. Hovmöller (Latitude vs Time) plot of the GOSAT Proxy XCH$_4$ (top), TM5 model XCH$_4$ (middle) and the GOSAT-TM5 difference (bottom). The model data has been sampled at the time/location of the GOSAT observation and had the sounding-specific GOSAT averaging kernel applied.

6 Global CH$_4$ Distributions

As discussed in Section 3, one of the primary applications for the GOSAT Proxy XCH$_4$ data has been as input to global flux inversions. For this reason, it is useful to examine the global spatio-temporal distribution of the data. Figure 10 shows seasonal maps of the GOSAT data from Spring (March/April/May) 2009 through to Winter (December) 2019. Features of note include:
5   a consistent increase in concentration over time; strong regional signals associated with CH$_4$ surface sources, particularly over South America, India, China and Africa; a clear seasonal cycle over many regions; and a significant increase in the number and latitudinal range of GOSAT ocean sun-glint observations from 2014/2015.

Despite changes in the GOSAT sampling pattern and various instrument issues resulting in data gaps (see Section 2.1), on a seasonal and global scale there is good data coverage throughout the entire decade of observations.

10   7 Model Comparisons

The purpose of this paper is to present details of the v9.0 Proxy dataset and provide information to facilitate the future use of the data. As such, it is not the intention that this work performs detailed scientific analysis and interpretation. We do not, for example perform any atmospheric flux inversions using this data as that is a significant study in its own right. However, we do feel that it would be informative to users of the data for us to perform a comparison against existing model XCH$_4$ simulations
15   to give confidence that the data is of sufficient quality to use in such studies.

In this section we compare the GOSAT Proxy XCH$_4$ data to a simulation of the TM5 global chemistry transport model (Bergamaschi et al., 2013, 2018b) which has assimilated NOAA surface measurements. We have chosen to compare against model simulations that are both widely used within the community and that have already assimilated NOAA surface measurements. The reasoning for this is that any overall differences as might be seen from free-running model simulation are removed and we
20   can clearly state the consistency of our dataset with the NOAA network. By proving good overall agreement to both TCCON

20
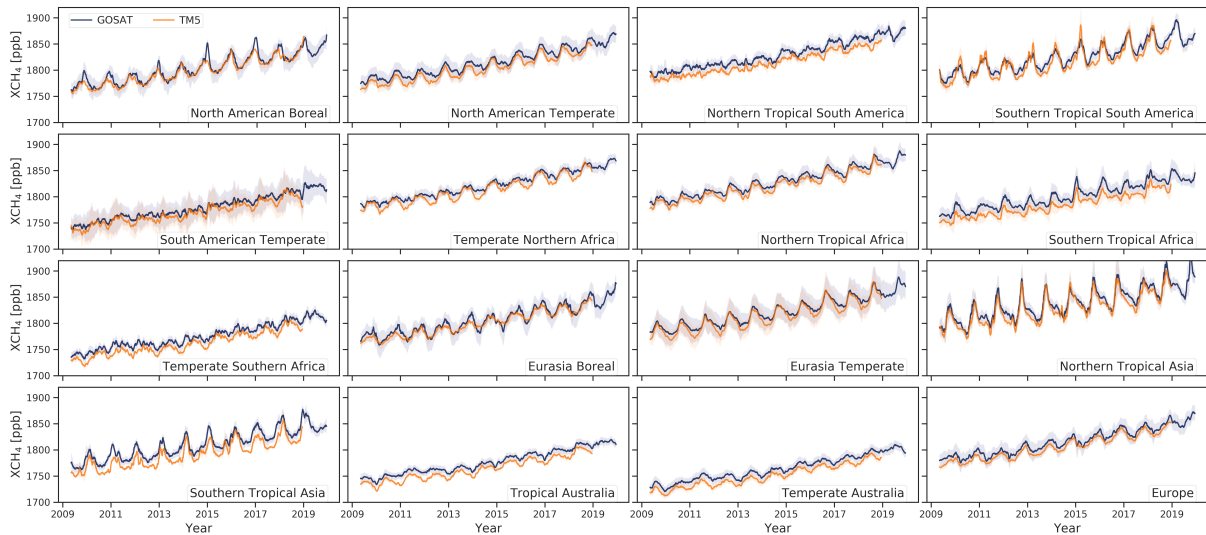
Figure 12. Time series comparison between the GOSAT Proxy XCH$_4$ data and TM5 model XCH$_4$ simulations (Bergamaschi et al., 2018b) for individual TransCom regions. The model data has been sampled at the time/location of the GOSAT observation and had the sounding-specific GOSAT averaging kernel applied.

measurements (Section 5) and the NOAA-constrained model simulations we believe this indicates the utility of our data for use in further scientific analysis. This model data is the same data as used in the *Global Methane Budget 2000-2017* (Saunois et al., 2020) and in that study is referred to as "TM5-4DVAR". For these comparisons, we have sampled the TM5 model at the time and location of the GOSAT measurement, interpolated the model to the GOSAT retrieval grid, applied the sounding-specific

5 GOSAT CH$_4$ averaging kernel (see Figure 1 and Appendix D) and computed the model total column XCH$_4$ amount.

Figure 11 shows Hovmöller plots (latitudinal mean versus time) for the GOSAT Proxy XCH$_4$ (top), TM5 model simulation (middle) and the GOSAT-TM5 difference (bottom). The GOSAT distribution behaves as expected, showing an increase over time between 2009 and 2019 superimposed on top of a north-south gradient and regular seasonal cycle. The TM5 data exhibits very similar characteristics and is in very good agreement to the GOSAT data. The difference between the two datasets (lower

10 panel) shows that although there is a small offset between the two (with GOSAT on average 6.55 ppb larger than the model), there is very good consistency over time. GOSAT and TM5 seem to agree slightly better during the peak of the seasonal cycle, particularly in the tropics, with the TM5 exhibiting a shallower trough. At very high northern latitudes, GOSAT is slightly lower than the model but this relates to observations over Greenland at high altitude and low signal to-noise ratio for the GOSAT soundings so care must be taken not to over-interpret this difference.

15 With Figure 11 providing confidence that the GOSAT data and TM5 simulation are in broad agreement, it is informative to break these comparisons down to a regional scale. Figure 12 shows timeseries of the GOSAT and TM5 data over the 16 different TRANSCOM regions (Gurney et al., 2002). All regions show good agreement between the modelled and observed data. We compute the de-seasonalised XCH$_4$ over time for each region. The average difference in model and observation ranges from

21

3.9 ppb (Eurasian Boreal) to 15.4 ppb (Southern Tropical Asia). On average across all regions, the mean difference between the model and observation is 9.8 ppb.

The observed seasonal cycles in each region are very well-represented by the model, with an average correlation coefficient of 0.93 (ranging from 0.84 to 0.98 across all regions). The peak to peak seasonal cycle timing and magnitude is very well reproduced between the two datasets. For example, the average peak to peak seasonal cycle amplitude for Northern Tropical Asia is 61.1 ppb for GOSAT and 62.3 ppb for TM5 whilst for North American Temperate it is 22.7 ppb for GOSAT and 23.6 ppb for TM5. The average GOSAT-model difference between the mean seasonal cycle amplitude across all regions is -0.84 ppb with the average absolute difference being 5.3 ppb with only a small number of instances where the model and observation strongly disagree (for example in North America Boreal and South America Tropical in 2015, likely indicative of isolated regional emissions).

It is not the purpose of this paper to diagnose or interpret detailed differences between the observations and model but it is useful to make a few observations relevant for use of the data within future studies. Figure 12 indicates a potential latitude-dependent bias, which is most likely due to model deficiencies in simulating the stratosphere (especially at mid and high latitudes ~~(Alexe et al., 2015; Wang et al., 2017)~~(Patra et al., 2011; Alexe et al., 2015; Saad et al., 2016; Wang et al., 2017)) or inadequate inter-hemispheric mixing, but could partly indicate also some latitudinal bias of the satellite retrievals. Accounting for such a latitudinal dependence through the fitting of a second-order polynomial function (as in ~~Bergamaschi et al. (2013)~~ Bergamaschi et al. (2013); Turner et al. (2015)) may improve the baseline agreement between model and observation and is an approach that users may wish to explore depending upon their application. Furthermore, these model simulations are constrained by the NOAA background observations. Therefore differences between TM5-4DVAR and GOSAT may partly reflect deficiencies of bottom-up inventories used as prior, particularly over strong emission regions (e.g. obvious deficiencies in tropical Africa related to wetlands). When incorporating the GOSAT data into such inversions, this leads to the production of significant increments in the inverted fluxes and better agreement between observation and simulation (as in Alexe et al. (2015) and other studies noted in Section 3.4).

8   Summary and Outlook

In this work we have presented the latest version of the University of Leicester GOSAT Proxy XCH$_4$ dataset. This dataset now contains over a decade of global CH$_4$ observations, sensitive to surface emissions and hence suited to estimating CH$_4$ fluxes. The capability to estimate global and regional CH$_4$ emissions is vital to improving our understanding of the global methane budget and how this budget may respond and change with respect to a changing future climate.

We begin this work by highlighting the wide variety of studies that previous versions of this dataset have contributed towards, demonstrating the significant utility of this dataset for examining and understanding the global methane budget.

This work provides a thorough description of the data processing chain, explaining in detail how the data is generated and how the high-quality of the dataset is ensured. Extensive validation of the data against the TCCON network is performed,

validating not only the final Proxy XCH$_4$ data but also the separate components (the XCH$_4$/XCO$_2$ ratio and the modelled XCO$_2$) that form the final data product.

We also provide global seasonal maps of the data that demonstrate the global distribution of the data as well as highlighting particular features and regions that may be of interest for more detailed study.

Finally, as the primary usage of the data is expected to be as input into a flux inversion data assimilation framework in conjunction with atmospheric chemistry transport models and observations from surface networks, it is useful to compare the consistency against existing model simulations. We compare zonally and regionally against TM5 simulations that have assimilated observations from the NOAA surface network. We find generally a high level of consistency whilst identifying the additional utility that the satellite observations should introduce to the system.

Despite GOSAT-1 having a planned mission lifetime of 5 years, it continues to successfully perform measurements 11 years after launch. GOSAT-2 was launched in October 2018 (Suto et al., 2020) and will continue the legacy of the GOSAT-1 mission. GOSAT-2 offers several opportunities for development related to the dataset we describe here. Primarily, it ensures that should GOSAT-1 cease operation, the valuable decade-long timeseries of observations can continue to be extended via GOSAT-2. With a significant overlap in time between the two missions, consistency between the two missions can be assured, albeit with significant future work/development.

In addition, GOSAT-2 has additional capabilities, namely the possibility of measuring carbon monoxide (CO). By measuring CO$_2$, CH$_4$ and CO simultaneously from the same instrument, GOSAT-2 would allow the extension of studies examining biomass burning combustion, leading to constraints on fire emission ratios as have been performed previously for GOSAT-1 (Ross et al., 2013; Parker et al., 2016).

A strong focus of future CH$_4$-measuring satellites will be to examine anthropogenic emission sources at very high spatial resolution (e.g. PRISMA (Pignatti et al., 2013); HISUI (Matsunaga et al., 2017); ENMAP (Guanter et al., 2015)), particularly relating to monitoring of the oil and gas industry. However, many scientific challenges and questions remain regarding the long-term CH$_4$ behaviour and the response to a changing climate. For this reason, a long-term, consistent climate-ready data record as we present here is of continued importance. We expect that this data will be valuable for numerous studies, from regional flux inversions to monitoring long-term trends. With now over a decade of global atmospheric XCH$_4$ observations, this dataset has helped, and will continue to help, us better understand the global methane budget and investigate how it may respond to a future changing climate.

9 Data availability

The University of Leicester GOSAT Proxy v9.0 XCH$_4$ data (Parker and Boesch, 2020) is available from the Centre for Environmental Data Analysis data repository at https://doi.org/10.5285/18ef8247f52a4cb6a14013f8235cc1eb. The TCCON data is available from the TCCON Data Archive at https://tccondata.org (individual data citations are provided in Table A1). CAMS model CO$_2$ (v18r2) data is available from the Copernicus Atmospheric Data Store at https://ads.atmosphere.copernicus.eu/cdsapp#!/dataset/cams-global-greenhouse-gas-inversion. MACC model CH$_4$ (v10-S1NOAA) is available from ECMWF at

https://apps.ecmwf.int/datasets/data/macc-ghg-inversions/. NOAA CarbonTracker model CO_2 (CT2017 and CT2019-NRT) are available from NOAA ESRL, Boulder, Colorado, USA at ftp://aftp.cmdl.noaa.gov/products/carbontracker/co2/.

Appendix A: Summary of Dataset Characteristics

Table A1 summarises the key characteristics of the University of Leicester GOSAT Proxy XCH₄ data, including the spatial and temporal extent that the dataset covers, the total number of measurements and their evaluation against TCCON.

Attribute	Value
Temporal Extent	2009-2019
Spatial Extent	Global (56.3°S - 83.5°N)
Total Number of Measurements	4.6 million
Footprint Size	10.5km (at nadir)
Overpass Time (at Equator)	∼13:00 Local Solar Time
Bias (vs TCCON)	0 ppb (after global bias correction of 9.06 ppb)
Precision (vs TCCON)	13.72 ppb

Table A1. Table summarising the key characteristics of the University of Leicester GOSAT Proxy XCH₄ data.

Appendix B: Previous Data Versions

Table B1 outlines the history and evolution of the University of Leicester GOSAT Proxy XCH₄ data product. Entries include the version number, the project that the data was generated for, the version of the GOSAT L1B data used, the time period covered by the data, whether ocean sun-glint data was generated, comments relating to changes/updates from previous versions and peer-reviewed publications that we are aware of that used the data. For the ESA GHG-CCI project, we also indicate which versions were officially delivered as part of the Climate Research Data Packages through the project. All Copernicus C3S versions were delivered to the Copernicus Climate Data Store.

Appendix C: Data Contents and Usage Notes

This section provides information on the contents and usage of the netCDF data files that we provide containing the Proxy XCH₄ data. Whilst we recommend that anyone using the data should discuss their specific usage with the author, the following information is useful to note.

Our data is delivered as daily netCDF files, containing `n` individual GOSAT soundings. We provide everything in the data files that we believe users would require to make use of our data, including our a priori information (`ch4_profile_apriori`) and averaging kernels (`xch4_averaging_kernel`) which are provided on `m` vertical levels (see Appendix D).

In general, users should **only use data that passes our quality checks (i.e. `xch4_quality_flag == 0`)**. In some specific use cases, the data that has failed our checks may still be of use but additional care should be taken in using this data and we strongly recommend discussing such applications with us to determine if that is suitable for your use.

25

Version	Project	L1B	Time Period	Ocean?	Comments	Publications Utilising Data
1.0	NCEO	006 007	2009-2010	No	First release.	Parker et al. (2011)
2.0	NCEO	050 080 100	2009-2010	No	Development version; only processed at TCCON overpasses; new radiometric calibration for L1B from JAXA applied.	
3.0	CCI	050 080 100	2009-2010	No	First version generated as part of ESA CCI Round Robin and Algorithm Intercomparison. Improvements to surface pressure calculation taking into account instrument field-of-view. Significant speed improvements to preprocessing steps to allow multi-year processing.	
3.1	CCI	050 080 100	2009-2010	No	Incremental updates and bug fixes.	
3.2	CCI	050 080 100	2009-2010	No	Incremental updates and bug fixes. First version to be used for atmospheric inversions.	Ross et al. (2013); Fraser et al. (2013); Dils et al. (2014); Wecht et al. (2014); Cressot et al. (2014); Berchet et al. (2015); Worden et al. (2015)
4.0	CCI CRDP1	141 150 151	2009-2011	No	First version that was widely released to scientific community via CCI. Change in CO_2 model from CarbonTracker to MACCII; tightening of stratospheric covariance; spectral degradation applied as per Yoshida et al. (2013); higher resolution ERA-Interim; variable vertical grid based on tropopause height.	Fraser et al. (2014); Turner et al. (2015); Alexe et al. (2015)
5.0	CCI	160 161	2009-2013	No	Introduction of model median XCO_2 with MACCII, CarbonTracker and GEOS-Chem (as per Parker at al, 2015); CH_4 prior combines MACCII (troposphere) and TOMCAT (stratosphere); SRTM DEM used for topography; updated GOSAT L1B degradation correction based on Kuze et al. (2014).	
5.1	CCI	160 161	2009-2013	No	Resolved minor issue with uncertainty variable in 5.0.	
5.2	CCI CRDP2	160 161	2009-2013	No	Resolved minor issue with pressure weighting function In 5.1.	Parker et al. (2015); Stanevich et al. (2019, 2020)
6.0	CCI CRDP3	160 161	2009-2014	Yes	Inclusion of ocean sun-glint observations for first time.	Webb et al. (2016); McNorton et al. (2016b); Siddans et al. (2017); Feng et al. (2017); Buchwitz et al. (2017b, 2018)
6.1	CCI	160 161	2009-2015	Yes	Temporal extension of 6.0.	Ganesan et al. (2017)
7.0	CCI CRDP4	201 202	2009-2015	Yes	New L1B data and updates to CO_2 models used in ensemble for Proxy calculation.	Parker et al. (2016, 2018); McNorton et al. (2018); Sheng et al. (2018); Maasakkers et al. (2019, 2020); Lunt et al. (2019)
7.0	C3S	201 202	2009-2016	Yes	Time period extended and first delivery to C3S. No changes to processing so retained version number.	
7.1	C3S	201 202 210	2009-2017	Yes	Extension of 7.0 with updated L1B for latter years.	
7.2	C3S	201 202 210	2009-2018	Yes	Extension of 7.1 with updated L1B for latter years.	Zheng et al. (2019); Reuter et al. (2020); Yin et al. (2020); Parker et al. (2020b); Saunois et al. (2020); Tunnicliffe et al. (2020)
8.0	C3S	210	2009-2018	Yes	Internal version for testing/development of new processing pipeline.	
9.0	C3S	210	2009-2019	Yes	**The dataset described in this publication.** Fully consistent timeseries. Uses new python-based preprocessing (LRPT).	Parker et al. (2020a); Lu et al. (2020); Zhang et al. (2020)

Table B1. Table showing the evolution of the University of Leicester GOSAT Proxy XCH_4 data product. Entries include the version number, the project that the data was generated for, the version of the GOSAT L1B data used, the time period covered by the data, whether ocean sun-glint data was generated, comments relating to changes/updates from previous versions and peer-reviewed publications that we are aware of that used the data. For the ESA GHG-CCI project, we also indicate which versions were officially delivered as part of the Climate Research Data Packages through the project. All Copernicus C3S versions were delivered to the Copernicus Climate Data Store.

We provide data from both observation modes (nadir land and ocean sun-glint) in the same file. While we do not believe that we have any bias between these different modes, for some use cases, users may wish to exclude either of these modes. `retr_flag` provides information on the mode for each sounding (`0 = land, 1 = glint`).

The variable named `xch4` refers to the final Proxy XCH$_4$ as calculated using Equation 1. **This is the main data product**
5 **that we provide.** In addition to this, we also provide the other components of Equation 1. `raw_xch4` and `raw_xco2` refer to the directly retrieved XCH$_4$ and XCO$_2$ quantities. These variables should generally not be used but may be useful for certain applications. For example, some users may wish to use the XCH$_4$/XCO$_2$ ratio (i.e. `raw_xch4/raw_xco2`) but replace the model XCO$_2$ that we use (`model_xco2`) with their own modelled XCO$_2$ which may be more appropriate to their particular application or more consistent with their own model transport.

10 Our retrievals are typically performed on 20 vertical levels, with the first (bottom) level being the surface pressure. However, in a number of instances, especially over high terrain, where the apparent surface pressure from our O$_2$-A band cloud screening is above the bottom two levels of our pressure profile, this can result in only 19 active retrieval levels. This data is still valid but variables with a vertical dimension (`m`) will contain a `fill_value` of -9999.99 at the first/lowest value. This value should be checked for and that particular profile should be considered to only have 19 levels, rather than the standard 20.

15 We identify individual GOSAT soundings by their `exposure_id`. This may be of use when attempting to match our data to other GOSAT data products. This is a numerical identification that matches the GOSAT L1B file which the sounding was extracted from, appended with an additional 3 digits (0-indexed) to identify the number of the sounding within that L1B file. Equation C1 shows the structure of the `exposure_id`. The `exposure_id` of `20090801004704401300006` was the 7th (`006`) sounding originating from the GOSAT L1B file named `GOSATTFTS20090801004704401300_1BOB1D210210.01`.

20 The nomenclature for the GOSAT L1B file includes year (`2009`), month (`08`), day (`01`), hour (`00`), minute (`47`), orbit (`044`), scene (`0130`). Note that these times are the times for the start of that GOSAT scene and not the exact measurement time. We provide the `time` variable as the measurement start time.

(C1)

27

Appendix D: Application of GOSAT Averaging Kernels to Model Data

In order to correctly compare any model simulation to the satellite observations, the model data must be transformed to be consistent with assumptions made within the retrieval. Ultimately, this requires the satellite averaging kernels to be applied to the model data with any influence from the a priori data taken into account. The theory and methodology to do this is
5 described in detail in Rodgers (2000) and we only briefly outline the method below. Equation D1 is the equation which should be applied to any CH_4 model data and details which variables provided in the data files are required to achieve this. It is assumed that any model data has already been interpolated to the same 20-level pressure grid (`pressure_levels`) as used in the retrieval. It should be noted here that this interpolation should be done with care to try and ensure that the model XCH_4 is conserved via the interpolation process. Once on the same vertical grid as the GOSAT a priori and averaging kernels, Equation
10 D1 can be applied to compute the modelled XCH_4 by using the `pressure_weight`, `xch4_averaging_kernel` and `ch4_profile_apriori` variables provided in the file. It should be noted that we provide these values for each individual GOSAT sounding and that these are all level (i.e. layer boundary) quantities.

retrieval averaging kernel for level i

(`xch4_averaging_kernel`)

retrieval prior profile CH_4 VMR

for level i

(`ch4_profile_apriori`)

$$XCH_4^{mod} = \sum_{i=0}^{N_{lev}} \left\{ \left[VMR_i^{apr} + \left(VMR_i^{mod} - VMR_i^{apr} \right) AK_i \right] h_i \right\} \tag{D1}$$

model CH_4 sampled

at pressure level i

pressure weight

for level i

(`pressure_weight`)

Appendix E: Considerations Regarding GOSAT Measurement Strategy and Changes Over Time

This section provides details on how the GOSAT measurement strategy has evolved over time. GOSAT initially operated primarily on a regular 5-point grid, revisiting the same grid point. This changed over time to a 3-point grid in order to reduce pointing uncertainty at the extreme angles when using the primary pointing mechanism. However, one consequence of a regular grid is that this resulted in a limited number of observations over some regions, especially islands, where the regular grid point
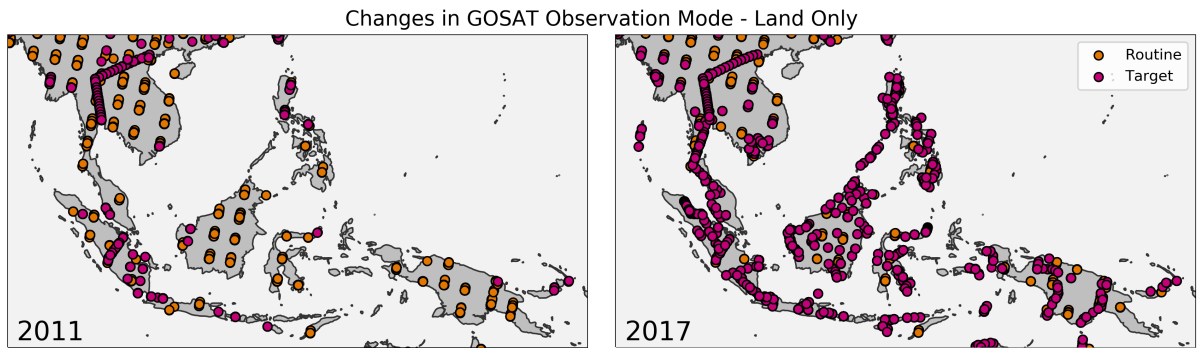
Figure E1. Figure contrasting the routine vs target observation modes for land-only measurements in 2011 and 2017 over Indonesia. The change in pointing mechanism has allowed a more sophisticated targeting strategy to optimise the number of land measurements over islands and coastlines.

would fall over the ocean. Thanks to the switch to the secondary pointing mechanism, several changes to the sampling strategy were possible.

Firstly, GOSAT is now capable of targeting more specifically and "follows" coastlines in a more efficient manner. The example in Figure E1 shows the change in sampling location over Indonesia, contrasting 2011 to 2017. Although the exact same grid location is not revisited in the same way, overall there are both more successful measurements and a better geographic coverage.

Secondly, GOSAT is now capable of a wider pointing range and subsequently, the latitudinal range of ocean sun-glint observations have been extended (as observed in Figure 10). Figure E2 provides example comparisons of the measurement density over Australia between the start of the mission (2009-2010) when the instrument was primarily operating in 5-point grid mode to the latter years (2018-2019) where the instrument is operating in 3-point grid mode, with extended latitudinal sun-glint coverage.

While we do not believe that these changes are detrimental to the continued consistency of the timeseries of GOSAT observations, we do feel that it is worth noting as they may have an impact (positively or negatively) on specific applications that a user may wish to use the data for, hence the reason for highlighting them here.
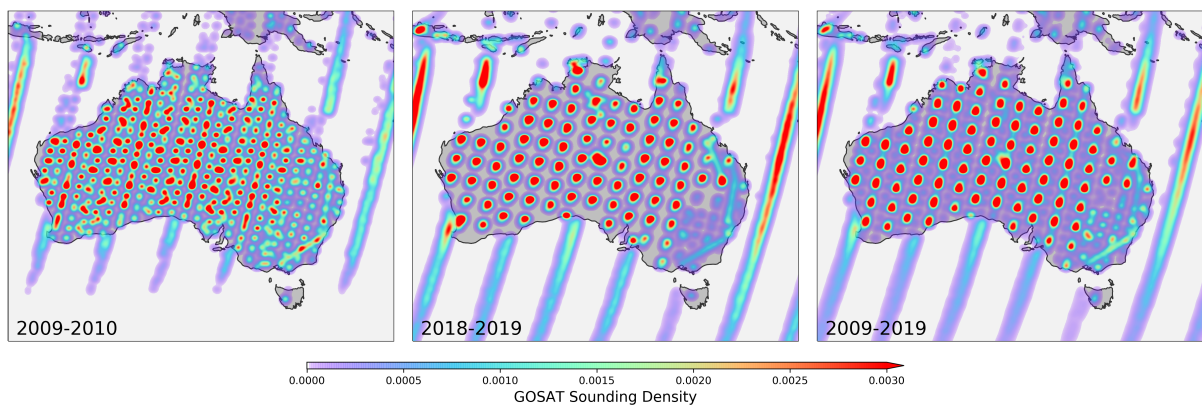
Figure E2. Figure contrasting the sampling density pattern over Australia for early in the mission versus recent years. The 5-point sampling grid as used in the early years of the missions was updated to a more stable 3-point grid which continues to be used. The change in pointing mechanism has allowed the ocean sun-glint measurement range to be extended.
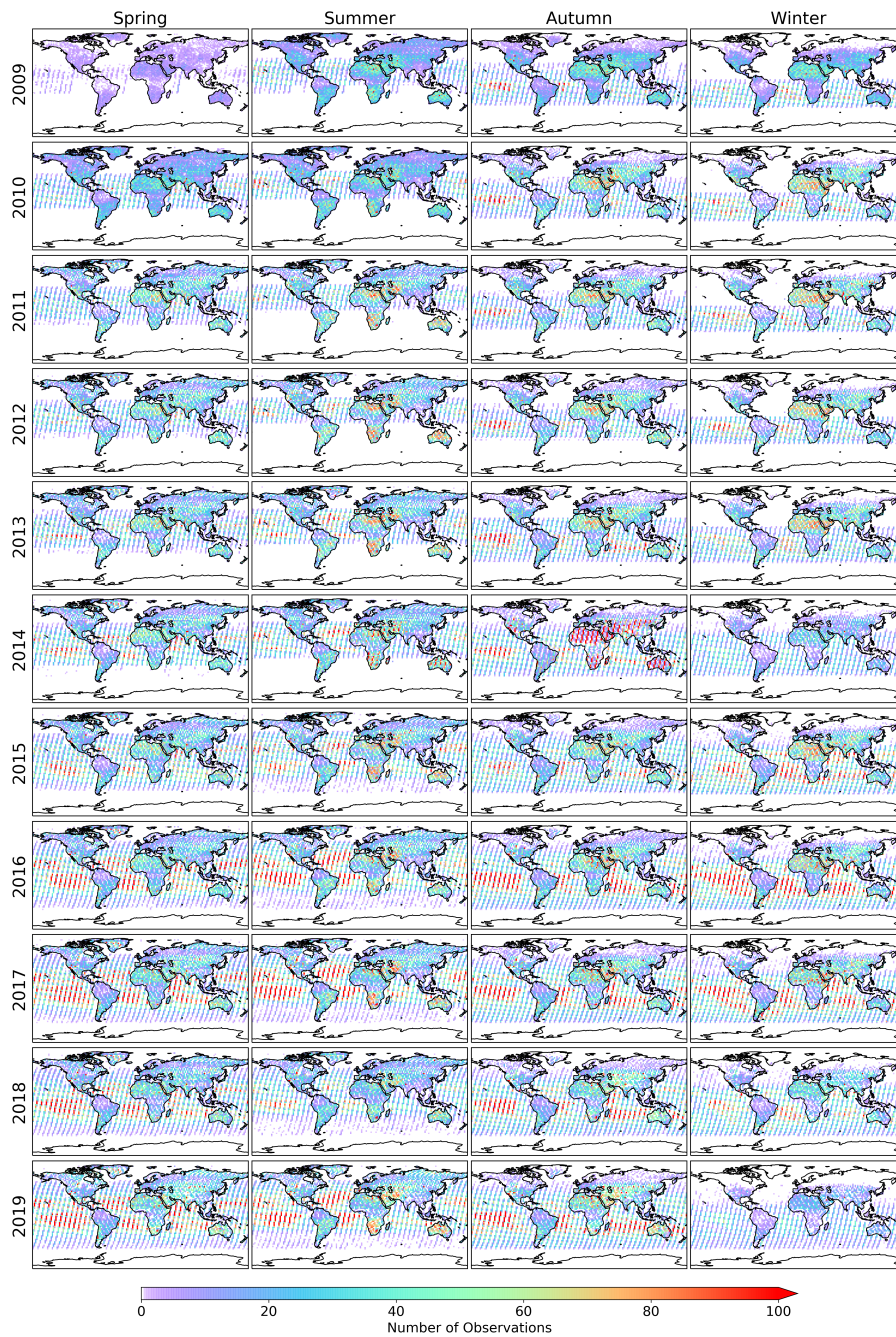
Figure E3. Figure showing the number of successful GOSAT XCH$_4$ measurements per 2° latitude-longitude bin for each year/season.

Appendix F: TCCON Data

The section provides details and references for the TCCON data used in this study. Table lists all of the TCCON sites used in the study, along with their latitude, when the data record begins and the citation to each specific dataset.

Site	Latitude	Established	Data Citation
Eureka	80.05°N	July 2010	Strong et al. (2019)
Sodankylä	67.37°N	January 2009	Kivi et al. (2014)
East Trout Lake	54.35°N	October 2016	Wunch et al. (2018)
Bialystok	53.23°N	March 2009	Deutscher et al. (2014)
Bremen	53.10°N	July 2004	Notholt et al. (2019)
Karlsruhe	49.10°N	September 2009	Hase et al. (2015)
Paris	48.85°N	September 2014	Té et al. (2014)
Orleans	47.97°N	August 2009	Warneke et al. (2014)
Garmisch	47.476°N	July 2007	Sussmann and Rettinger (2018)
Park Falls	45.95°N	May 2004	Wennberg et al. (2017)
Rikubetsu	43.46°N	November 2013	Morino et al. (2018c)
Lamont	36.60°N	July 2008	Wennberg et al. (2016)
Anmyeondo	36.5°N	August 2014	Goo et al. (2014)
Tsukuba (125HR)	36.05°N	December 2008	Morino et al. (2018a)
Saga	33.24°N	June 2011	Shiomi et al. (2014)
Burgos	18.53°N	March 2017	Morino et al. (2018b)
Ascension Island	7.92°S	May 2012	Feist et al. (2014)
Darwin	12.42°S	August 2005	Griffith et al. (2014a)
Reunion Island	20.90°S	September 2011	De Maziere et al. (2017)
Wollongong	34.41°S	May 2008	Griffith et al. (2014b)
Lauder (125 HR)	45.04°S	February 2010	Sherlock et al. (2014b)
Lauder (120 HR)	45.04°S	June 2004	Sherlock et al. (2014a)

Table A1. The TCCON sites used in this study, along with their latitude, when they were established and the citation to the data used.

References

Alexe, M., Bergamaschi, P., Segers, A., Detmers, R., Butz, A., Hasekamp, O., Guerlet, S., Parker, R., Boesch, H., Frankenberg, C., Scheepmaker, R. A., Dlugokencky, E., Sweeney, C., Wofsy, S. C., and Kort, E. A.: Inverse modelling of CH_4 emissions for 2010-2011 using different satellite retrieval products from GOSAT and SCIAMACHY, Atmospheric Chemistry and Physics, 15, 113–133, https://doi.org/10.5194/acp-15-113-2015, 2015.

5

Berchet, A., Pison, I., Chevallier, F., Paris, J.-D., Bousquet, P., Bonne, J.-L., Arshinov, M. Y., Belan, B. D., Cressot, C., Davydov, D. K., Dlugokencky, E. J., Fofonov, A. V., Galanin, A., Lavrič, J., Machida, T., Parker, R., Sasakawa, M., Spahni, R., Stocker, B. D., and Winderlich, J.: Natural and anthropogenic methane fluxes in Eurasia: a mesoscale quantification by generalized atmospheric inversion, Biogeosciences, 12, 5393–5414, https://doi.org/10.5194/bg-12-5393-2015, 2015.

10

Bergamaschi, P., Houweling, S., Segers, A., Krol, M., Frankenberg, C., Scheepmaker, R. A., Dlugokencky, E., Wofsy, S. C., Kort, E. A., Sweeney, C., Schuck, T., Brenninkmeijer, C., Chen, H., Beck, V., and Gerbig, C.: Atmospheric CH_4 in the first decade of the 21st century: Inverse modeling analysis using SCIAMACHY satellite retrievals and NOAA surface measurements, Journal of Geophysical Research: Atmospheres, 118, 7350–7369, https://doi.org/10.1002/jgrd.50480, 2013.

Bergamaschi, P., Danila, A., Weiss, R. F., Ciais, P., Thompson, R. L., Brunner, D., Levin, I., Meijer, Y., Chevallier, F., Bovensmann, H.,

15

Crisp, D., Basu, S., Dlugokencky, E., Engelen, R., Gerbig, C., Günther, D., Hammer, S., Henne, S., Houweling, S., Peylin, P., Pinty, B., Ramonet, M., Reimann, S., Röckmann, T., Schmidt, M., Strogies, M., Sussams, J., Tarasova, O., van Aardenne, J., Vermeulen, A. T., and Vogel, F.: Atmospheric monitoring and inverse modelling for verification of greenhouse gas inventories, EUR 29276 EN, Publications Office of the European Union, Luxembourg, https://doi.org/10.2760/759928, 2018a.

Bergamaschi, P., Karstens, U., Manning, A. J., Saunois, M., Tsuruta, A., Berchet, A., Vermeulen, A. T., Arnold, T., Janssens-Maenhout,

20

G., Hammer, S., Levin, I., Schmidt, M., Ramonet, M., Lopez, M., Lavric, J., Aalto, T., Chen, H., Feist, D. G., Gerbig, C., Haszpra, L., Hermansen, O., Manca, G., Moncrieff, J., Meinhardt, F., Necki, J., Galkowski, M., O'Doherty, S., Paramonova, N., Scheeren, H. A., Steinbacher, M., and Dlugokencky, E.: Inverse modelling of European CH_4 emissions during 2006-2012 using different inverse models and reassessed atmospheric observations, Atmospheric Chemistry and Physics, 18, 901–920, https://doi.org/10.5194/acp-18-901-2018, 2018b.

25

Boesch, H., Baker, D., Connor, B., Crisp, D., and Miller, C.: Global Characterization of CO_2 Column Retrievals from Shortwave-Infrared Satellite Observations of the Orbiting Carbon Observatory-2 Mission, Remote Sensing, 3, 270–304, https://doi.org/10.3390/rs3020270, 2011.

Buchwitz, M., Reuter, M., Schneising, O., Hewson, W., Detmers, R. G., Boesch, H., Hasekamp, O. P., Aben, I., Bovensmann, H., Burrows, J. P., Butz, A., Chevallier, F., Dils, B., Frankenberg, C., Heymann, J., Lichtenberg, G., De Mazière, M., Notholt, J., Parker, R.,

30

Warneke, T., Zehner, C., Griffith, D. W. T., Deutscher, N. M., Kuze, A., Suto, H., and Wunch, D.: Global satellite observations of column-averaged carbon dioxide and methane: The GHG-CCI XCO2 and XCH4 CRDP3 data set, Remote Sensing of Environment, 203, 276–295, https://doi.org/10.1016/j.rse.2016.12.027, 2017a.

Buchwitz, M., Schneising, O., Reuter, M., Heymann, J., Krautwurst, S., Bovensmann, H., Burrows, J. P., Boesch, H., Parker, R. J., Somkuti, P., Detmers, R. G., Hasekamp, O. P., Aben, I., Butz, A., Frankenberg, C., and Turner, A. J.: Satellite-derived methane hotspot emission

35

estimates using a fast data-driven method, Atmospheric Chemistry and Physics, 17, 5751–5774, https://doi.org/10.5194/acp-17-5751-2017, 2017b.

Buchwitz, M., Reuter, M., Schneising, O., Bovensmann, H., Burrows, J. P., Boesch, H., Anand, J., Parker, R., Detmers, R. G., Aben, I., Hasekamp, O. P., Crevoisier, C., Armante, R., Zehner, C., and Schepers, D.: Copernicus Climate Change Service (C3S) global satellite observations of atmospheric carbon dioxide and methane, Proceedings of the International Astronautical Congress, IAC, 2018-Octob, 57–60, https://doi.org/10.1007/s42423-018-0004-6, 2018.

5 Butz, A., Hasekamp, O. P., Frankenberg, C., Vidot, J., and Aben, I.: CH_4 retrievals from space-based solar backscatter measurements: Performance evaluation against simulated aerosol and cirrus loaded scenes, Journal of Geophysical Research D: Atmospheres, 115, https://doi.org/10.1029/2010JD014514, 2010.

Chevallier, F.: Documentation of the CO_2 flux service: Description of the CO_2 inversion production, Tech. rep., European Centre for Medium-Range Weather Forecasts, 2019.

10 Chevallier, F., Feng, L., Bösch, H., Palmer, P. I., and Rayner, P. J.: On the impact of transport model errors for the estimation of CO_2 surface fluxes from GOSAT observations, Geophysical Research Letters, 37, https://doi.org/10.1029/2010GL044652, 2010.

Chipperfield, M. P.: Multiannual simulations with a three-dimensional chemical transport model, Journal of Geophysical Research: Atmospheres, 104, 1781–1805, https://doi.org/10.1029/98JD02597, 1999.

Cogan, A. J., Boesch, H., Parker, R. J., Feng, L., Palmer, P. I., Blavier, J.-F. L. F., Deutscher, N. M., MacAtangay, R., Notholt, J., Roehl, C.,

15 Warneke, T., and Wunch, D.: Atmospheric carbon dioxide retrieved from the Greenhouse gases Observing SATellite (GOSAT): Comparison with ground-based TCCON observations and GEOS-Chem model calculations, Journal of Geophysical Research Atmospheres, 117, n/a–n/a, https://doi.org/10.1029/2012JD018087, 2012.

Connor, B. J., Boesch, H., Toon, G., Sen, B., Miller, C., and Crisp, D.: Orbiting Carbon Observatory: Inverse method and prospective error analysis, Journal of Geophysical Research D: Atmospheres, 113, https://doi.org/10.1029/2006JD008336, 2008.

20 Cressot, C., Chevallier, F., Bousquet, P., Crevoisier, C., Dlugokencky, E. J., Fortems-Cheiney, A., Frankenberg, C., Parker, R., Pison, I., Scheepmaker, R. A., Montzka, S. A., Krummel, P. B., Steele, L. P., and Langenfelds, R. L.: On the consistency between global and regional methane emissions inferred from SCIAMACHY, TANSO-FTS, IASI and surface measurements, Atmospheric Chemistry and Physics, 14, 577–592, https://doi.org/10.5194/acp-14-577-2014, 2014.

De Mazière, M., Barret, B., Blumenstock, T., Buchwitz, M., De Beek, R., Demoulin, P., Fast, H., Gloudemans, A., Griesfeller, A., Griffith,

25 D., Ionov, D., Janssens, K., Jones, N., Mahieu, E., Mellqvist, J., Mittermeier, R. L., Notholt, J., Rinsland, C., Schrijver, H., Schultz, A., Smale, D., Strandberg, A., Strong, K., Sussmann, R., Warneke, T., and Wood, S.: Comparisons between sciamachy scientific products and ground-based FTIR data for total columns of CO, CH_4 and N_2O, European Space Agency, (Special Publication) ESA SP, pp. 89–96, https://doi.org/10.5194/acp-6-1953-2006, 2004.

De Maziere, M., Sha, M. K., Desmet, F., Hermans, C., Scolas, F., Kumps, N., Metzger, J.-M., Duflot, V., and Cam-

30 mas, J.-P.: TCCON data from Réunion Island (RE), Release GGG2014.R0, TCCON Data Archive, hosted by CaltechDATA, https://doi.org/10.14291/tccon.ggg2014.reunion01.R1, 2017.

Dee, D. P., Uppala, S. M., Simmons, A. J., Berrisford, P., Poli, P., Kobayashi, S., Andrae, U., Balmaseda, M. A., Balsamo, G., Bauer, P., Bechtold, P., Beljaars, A. C. M., van de Berg, L., Bidlot, J., Bormann, N., Delsol, C., Dragani, R., Fuentes, M., Geer, A. J., Haimberger, L., Healy, S. B., Hersbach, H., Hólm, E. V., Isaksen, L., Kållberg, P., Köhler, M., Matricardi, M., McNally, A. P., Monge-Sanz,

35 B. M., Morcrette, J.-J., Park, B.-K., Peubey, C., de Rosnay, P., Tavolato, C., Thépaut, J.-N., and Vitart, F.: The ERA-Interim reanalysis: configuration and performance of the data assimilation system, Quarterly Journal of the Royal Meteorological Society, 137, 553–597, https://doi.org/10.1002/qj.828, 2011.

Deutscher, N., Notholt, J., Messerschmidt, J., Weinzierl, C., Warneke, T., Petri, C., Grupe, P., and Katrynski, K.: TCCON data from Bialystok, Poland, Release GGG2014R2, TCCON data archive, hosted by CaltechDATA, https://doi.org/10.14291/tccon.ggg2014.bialystok01.R2, 2014.

Dils, B., De Maziere, M., Muller, J. F., Blumenstock, T., Buchwitz, M., De Beek, R., Demoulin, P., Duchatelet, P., Fast, H., Frankenberg, C., Gloudemans, A., Griffith, D., Jones, N., Kerzenmacher, T., Kramer, I., Mahieu, E., Mellqvist, J., Mittermeier, R. L., Notholt, J., Rinsland, C. P., Schrijver, H., Smale, D., Strandberg, A., Straume, A. G., Stremme, W., Strong, K., Sussmann, R., Taylor, J., Van Den Broek, M., Velazco, V., Wagner, T., Warneke, T., Wiacek, A., and Wood, S.: Comparisons between SCIAMACHY and ground-based FTIR data for total columns of CO, CH_4, CO_2 and N_2O, Atmospheric Chemistry and Physics, 6, 1953–1976, https://doi.org/10.5194/acp-6-1953-2006, 2006.

Dils, B., Buchwitz, M., Reuter, M., Schneising, O., Boesch, H., Parker, R., Guerlet, S., Aben, I., Blumenstock, T., Burrows, J. P., Butz, A., Deutscher, N. M., Frankenberg, C., Hase, F., Hasekamp, O. P., Heymann, J., De Mazière, M., Notholt, J., Sussmann, R., Warneke, T., Griffith, D., Sherlock, V., and Wunch, D.: The greenhouse gas climate change initiative (GHG-CCI): Comparative validation of GHG-CCI SCIAMACHY/ENVISAT and TANSO-FTS/GOSAT CO_2 and CH_4 retrieval algorithm products with measurements from the TCCON, Atmospheric Measurement Techniques, 7, 1723–1744, https://doi.org/10.5194/amt-7-1723-2014, 2014.

Dlugokencky, E. J., Bruhwiler, L., White, J. W. C., Emmons, L. K., Novelli, P. C., Montzka, S. A., Masarie, K. A., Lang, P. M., Crotwell, A. M., Miller, J. B., and Gatti, L. V.: Observational constraints on recent increases in the atmospheric CH_4 burden, Geophysical Research Letters, 36, https://doi.org/10.1029/2009GL039780, 2009.

Etminan, M., Myhre, G., Highwood, E. J., and Shine, K. P.: Radiative forcing of carbon dioxide, methane, and nitrous oxide: A significant revision of the methane radiative forcing, Geophysical Research Letters, 43, 12,614–12,623, https://doi.org/10.1002/2016GL071930, 2016.

Feist, D. G., Arnold, S. G., John, N., and Geibel, M. C.: TCCON data from Ascension Island, Saint Helena, Ascension and Tristan da Cunha, Release GGG2014R0, TCCON data archive, hosted by CaltechDATA, https://doi.org/10.14291/tccon.ggg2014.ascension01.r0/1149285, 2014.

Feng, L., Palmer, P. I., Yang, Y., Yantosca, R. M., Kawa, S. R., Paris, J.-D., Matsueda, H., and Machida, T.: Evaluating a 3-D transport model of atmospheric CO_2 using ground-based, aircraft, and space-borne data, Atmospheric Chemistry and Physics, 11, 2789–2803, https://doi.org/10.5194/acp-11-2789-2011, 2011.

Feng, L., Palmer, P. I., Bösch, H., Parker, R. J., Webb, A. J., Correia, C. S. C., Deutscher, N. M., Domingues, L. G., Feist, D. G., Gatti, L. V., Gloor, E., Hase, F., Kivi, R., Liu, Y., Miller, J. B., Morino, I., Sussmann, R., Strong, K., Uchino, O., Wang, J., and Zahn, A.: Consistent regional fluxes of CH_4 and CO_2 inferred from GOSAT proxy XCH_4:XCO_2 retrievals, 2010-2014, Atmospheric Chemistry and Physics, https://doi.org/10.5194/acp-17-4781-2017, 2017.

Frankenberg, C., Meirink, J. F., Bergamaschi, P., Goede, A. P. H., Heimann, M., Körner, S., Platt, U., van Weele, M., and Wagner, T.: Satellite chartography of atmospheric methane from SCIAMACHY on board ENVISAT: Analysis of the years 2003 and 2004, Journal of Geophysical Research: Atmospheres, 111, https://doi.org/10.1029/2005JD006235, 2006.

Fraser, A., Palmer, P. I., Feng, L., Boesch, H., Cogan, A., Parker, R., Dlugokencky, E. J., Fraser, P. J., Krummel, P. B., Langenfelds, R. L., O'Doherty, S., Prinn, R. G., Steele, L. P., van der Schoot, M., and Weiss, R. F.: Estimating regional methane surface fluxes: the relative importance of surface and GOSAT mole fraction measurements, Atmospheric Chemistry and Physics, 13, 5697–5713, https://doi.org/10.5194/acp-13-5697-2013, 2013.

Fraser, A., Palmer, P. I., Feng, L., Bösch, H., Parker, R., Dlugokencky, E. J., Krummel, P. B., and Langenfelds, R. L.: Estimating regional fluxes of CO_2 and CH_4 using space-borne observations of XCH_4: XCO_2, Atmospheric Chemistry and Physics, 14, 12 883–12 895, https://doi.org/10.5194/acp-14-12883-2014, 2014.

Ganesan, A. L., Rigby, M., Lunt, M. F., Parker, R. J., Boesch, H., Goulding, N., Umezawa, T., Zahn, A., Chatterjee, A., Prinn, R. G., Tiwari, Y. K., Van Der Schoot, M., and Krummel, P. B.: Atmospheric observations show accurate reporting and little growth in India's methane emissions, Nature Communications, 8, 836, https://doi.org/10.1038/s41467-017-00994-7, 2017.

Goo, T. Y., Oh, Y. S., and Velazco, V. A.: TCCON data from Anmyeondo (KOR), Release GGG2014R0, TCCON data archive, hosted by CaltechDATA, https://doi.org/10.14291/tccon.ggg2014.anmeyondo01.R0/1149284, 2014.

Griffith, D. W. T., Deutscher, N., Velazco, V. A., Wennberg, P. O., Yavin, Y., Keppel Aleks, G., Washenfelder, R., Toon, G. C., Blavier, J.-F., Murphy, C., Jones, N., Kettlewell, G., Connor, B., Macatangay, R., Roehl, C., Ryczek, M., Glowacki, J., Culgan, T., and Bryant, G.: TCCON data from Darwin (AU), Release GGG2014.R0, TCCON Data Archive, hosted by CaltechDATA, https://doi.org/10.14291/tccon.ggg2014.darwin01.R0/1149290, 2014a.

Griffith, D. W. T., Velazco, V. A., Deutscher, N., Murphy, C., Jones, N., Wilson, S., Macatangay, R., Kettlewell, G., Buchholz, R. R., and Riggenbach, M.: TCCON data from Wollongong (AU), Release GGG2014.R0, TCCON Data Archive, hosted by CaltechDATA, https://doi.org/10.14291/tccon.ggg2014.wollongong01.R0/1149291, 2014b.

Guanter, L., Kaufmann, H., Segl, K., Foerster, S., Rogass, C., Chabrillat, S., Kuester, T., Hollstein, A., Rossner, G., Chlebek, C., Straif, C., Fischer, S., Schrader, S., Storch, T., Heiden, U., Mueller, A., Bachmann, M., Mühle, H., Müller, R., Habermeyer, M., Ohndorf, A., Hill, J., Buddenbaum, H., Hostert, P., Van Der Linden, S., Leitão, P. J., Rabe, A., Doerffer, R., Krasemann, H., Xi, H., Mauser, W., Hank, T., Locherer, M., Rast, M., Staenz, K., and Sang, B.: The EnMAP spaceborne imaging spectroscopy mission for earth observation, Remote Sensing, 7, 8830–8857, https://doi.org/10.3390/rs70708830, 2015.

Gurney, K. R., Law, R. M., Denning, A. S., Rayner, P. J., Baker, D., Bousquet, P., Bruhwiler, L., Chen, Y.-H., Clals, P., Fan, S., Fung, I. Y., Gloor, M., Heimann, M., Higuchi, K., John, J., Maki, T., Maksyutov, S., Masarie, K., Peylin, P., Prather, M., Pak, B. C., Randerson, J., Sarmiento, J., Taguchi, S., Takahashi, T., and Yuen, C.-W.: Towards robust regional estimates of CO_2 sources and sinks using atmospheric transport models, Nature, 415, 626–630, https://doi.org/10.1038/415626a, 2002.

Hase, F., Blumenstock, T., Dohe, S., Groß, J., and Kiel, M.: TCCON data from Karlsruhe (DE), Release GGG2014.R1, TCCON Data Archive, hosted by CaltechDATA, https://doi.org/10.14291/tccon.ggg2014.karlsruhe01.R1/1182416, 2015.

Hausmann, P., Sussmann, R., and Smale, D.: Contribution of oil and natural gas production to renewed increase in atmospheric methane (2007-2014): Top-down estimate from ethane and methane column observations, Atmospheric Chemistry and Physics, 16, 3227–3244, https://doi.org/10.5194/acp-16-3227-2016, 2016.

Hu, H., Landgraf, J., Detmers, R., Borsdorff, T., Aan de Brugh, J., Aben, I., Butz, A., and Hasekamp, O.: Toward Global Mapping of Methane With TROPOMI: First Results and Intersatellite Comparison to GOSAT, Geophysical Research Letters, https://doi.org/10.1002/2018GL077259, 2018.

Inoue, M., Morino, I., Uchino, O., Nakatsuru, T., Yoshida, Y., Yokota, T., Wunch, D., Wennberg, P. O., Roehl, C. M., Griffith, D. W., Velazco, V. A., Deutscher, N. M., Warneke, T., Notholt, J., Robinson, J., Sherlock, V., Hase, F., Blumenstock, T., Rettinger, M., Sussmann, R., Kyrö, E., Kivi, R., Shiomi, K., Kawakami, S., De Mazière, M., Arnold, S. G., Feist, D. G., Barrow, E. A., Barney, J., Dubey, M., Schneider, M., Iraci, L. T., Podolske, J. R., Hillyard, P. W., Machida, T., Sawa, Y., Tsuboi, K., Matsueda, H., Sweeney, C., Tans, P. P., Andrews, A. E., Biraud, S. C., Fukuyama, Y., Pittman, J. V., Kort, E. A., and Tanaka, T.: Bias corrections of GOSAT SWIR XCO_2 and XCH_4 with TCCON

data and their evaluation using aircraft measurement data, Atmospheric Measurement Techniques, https://doi.org/10.5194/amt-9-3491-2016, 2016.

Jacob, D. J., Turner, A. J., Maasakkers, J. D., Sheng, J., Sun, K., Liu, X., Chance, K., Aben, I., McKeever, J., and Frankenberg, C.: Satellite observations of atmospheric methane and their value for quantifying methane emissions, Atmospheric Chemistry and Physics, 16, https://doi.org/10.5194/acp-16-14371-2016, 2016.

Kirschke, S., Bousquet, P., Ciais, P., Saunois, M., Canadell, J. G., Dlugokencky, E. J., Bergamaschi, P., Bergmann, D., Blake, D. R., Bruhwiler, L., et al.: Three decades of global methane sources and sinks, Nature Geoscience, 6, 813–823, https://doi.org/10.1038/ngeo1955, 2013.

Kivi, R., Heikkinen, P., and Kyro, E.: TCCON data from Sodankyla (FI), Release GGG2014R0, TCCON data archive, hosted by Caltech-DATA, https://doi.org/10.14291/tccon.ggg2014.sodankyla01.R0/1149280, 2014.

Kuze, A., Suto, H., Nakajima, M., and Hamazaki, T.: Thermal and near infrared sensor for carbon observation Fourier-transform spectrometer on the Greenhouse Gases Observing Satellite for greenhouse gases monitoring, Applied Optics, 48, 6716–6733, https://doi.org/10.1364/AO.48.006716, 2009.

Kuze, A., Taylor, T. E., Kataoka, F., Bruegge, C. J., Crisp, D., Harada, M., Helmlinger, M., Inoue, M., Kawakami, S., Kikuchi, N., Mitomi, Y., Murooka, J., Naitoh, M., O'Brien, D. M., O'Dell, C. W., Ohyama, H., Pollock, H., Schwandner, F. M., Shiomi, K., Suto, H., Takeda, T., Tanaka, T., Urabe, T., Yokota, T., and Yoshida, Y.: Long-Term Vicarious Calibration of GOSAT Short-Wave Sensors: Techniques for Error Reduction and New Estimates of Radiometric Degradation Factors, IEEE Transactions on Geoscience and Remote Sensing, 52, 3991–4004, 2014.

Kuze, A., Suto, H., Shiomi, K., Kawakami, S., Tanaka, M., Ueda, Y., Deguchi, A., Yoshida, J., Yamamoto, Y., Kataoka, F., Taylor, T. E., and Buijs, H.: Update on GOSAT TANSO-FTS performance, operations, and data products after more than six years in space, Atmospheric Measurement Techniques Discussions, 2016, 1–38, https://doi.org/10.5194/amt-2015-333, 2016.

Lambert, J.-C., Keppens, A., Hubert, D., Langerock, B., Eichmann, K.-U., Kleipool, Q., Sneep, M., Verhoelst, T., Wagner, T., Weber, M., Ahn, C., Argyrouli, A., Balis, D., Chan, K., Compernolle, S., Smedt, I. D., Eskes, H., Fjæraa, A., K. Garane, J. G., Gouta, F., and Wang, P.: Sentinel-5 Precursor Mission Performance Centre Quarterly Validation Report of the Copernicus Sentinel-5 Precursor Operational Data Products # 03 : July 2018 – May 2019, 2019.

Lu, X., Jacob, D. J., Zhang, Y., Maasakkers, J. D., Sulprizio, M. P., Shen, L., Qu, Z., Scarpelli, T. R., Nesser, H., Yantosca, R. M., Sheng, J., Andrews, A., Parker, R. J., Boech, H., Bloom, A. A., and Ma, S.: Global methane budget and trend, 2010–2017: complementarity of inverse analyses using in situ (GLOBALVIEWplus CH_4 ObsPack) and satellite (GOSAT) observations, Atmospheric Chemistry and Physics Discussions, 2020, 1–39, https://doi.org/10.5194/acp-2020-775, 2020.

Lunt, M. F., Palmer, P. I., Feng, L., Taylor, C. M., Boesch, H., and Parker, R. J.: An increase in methane emissions from tropical Africa between 2010 and 2016 inferred from satellite data, Atmospheric Chemistry and Physics Discussions, pp. 1–30, https://doi.org/10.5194/acp-2019-477, 2019.

Maasakkers, J. D., Jacob, D. J., Sulprizio, M. P., Scarpelli, T. R., Nesser, H., Sheng, J. X., Zhang, Y., Hersher, M., Anthony Bloom, A., Bowman, K. W., Worden, J. R., Janssens-Maenhout, G., and Parker, R. J.: Global distribution of methane emissions, emission trends, and OH concentrations and trends inferred from an inversion of GOSAT satellite data for 2010-2015, Atmospheric Chemistry and Physics, 19, 7859–7881, https://doi.org/10.5194/acp-19-7859-2019, 2019.

Maasakkers, J. D., Jacob, D. J., Sulprizio, M. P., Scarpelli, T. R., Nesser, H., Sheng, J., Zhang, Y., Lu, X., Bloom, A. A., Bowman, K. W., Worden, J. R., and Parker, R. J.: 2010–2015 North American methane emissions, sectoral contributions, and trends: a high-

resolution inversion of GOSAT satellite observations of atmospheric methane, Atmospheric Chemistry and Physics Discussions, 2020, 1–28, https://doi.org/10.5194/acp-2020-915, 2020.

Matsunaga, T., Iwasaki, A., Tsuchida, S., Iwao, K., Tanii, J., Kashimura, O., Nakamura, R., Yamamoto, H., Kato, S., Obata, K., Mouri, K., and Tachikawa, T.: Current status of Hyperspectral Imager Suite (HISUI) onboard International Space Station (ISS), in: 2017 IEEE International Geoscience and Remote Sensing Symposium (IGARSS), pp. 443–446, https://doi.org/10.1109/IGARSS.2017.8126989, 2017.

McNorton, J., Chipperfield, M. P., Gloor, M., Wilson, C., Feng, W., Hayman, G. D., Rigby, M., Krummel, P. B., O'Doherty, S., Prinn, R. G., Weiss, R. F., Young, D., Dlugokencky, E., and Montzka, S. A.: Role of OH variability in the stalling of the global atmospheric CH_4 growth rate from 1999 to 2006, Atmospheric Chemistry and Physics, 16, 7943–7956, https://doi.org/10.5194/acp-16-7943-2016, 2016a.

McNorton, J., Gloor, E., Wilson, C., Hayman, G. D., Gedney, N., Comyn-Platt, E., Marthews, T., Parker, R. J., Boesch, H., and Chipperfield, M. P.: Role of regional wetland emissions in atmospheric methane variability, Geophysical Research Letters, 43, 11,411–433,444, https://doi.org/10.1002/2016GL070649, 2016b.

McNorton, J., Wilson, C., Gloor, M., Parker, R. J., Boesch, H., Feng, W., Hossaini, R., and Chipperfield, M. P.: Attribution of recent increases in atmospheric methane through 3-D inverse modelling, Atmospheric Chemistry and Physics, 18, 18 149–18 168, https://doi.org/10.5194/acp-18-18149-2018, 2018.

Morino, I., Matsuzaki, T., and Horikawa, M.: TCCON data from Tsukuba (JP), 125HR, Release GGG2014.R2, TCCON Data Archive, hosted by CaltechDATA, https://doi.org/10.14291/tccon.ggg2014.tsukuba02.R2, 2018a.

Morino, I., Velazco, V. A., Hori, A., Uchino, O., and Griffith, D. W.: TCCON data from Burgos, Ilocos Norte (PH), Release GGG2014.R0, TCCON Data Archive, hosted by CaltechDATA, https://doi.org/10.14291/tccon.ggg2014.burgos01.R0, 2018b.

Morino, I., Yokozeki, N., Matzuzaki, T., and Shishime, A.: TCCON data from Rikubetsu (JP), Release GGG2014.R2, TCCON Data Archive, hosted by CaltechDATA, https://doi.org/10.14291/tccon.ggg2014.rikubetsu01.R2, 2018c.

Myhre, G., Shindell, D., Bréon, F.-M., Collins, W., Fuglestvedt, J., Huang, J., Koch, D., Lamarque, J.-F., Lee, D., Mendoza, B., Nakajima, T., Robock, A., Stephens, G., Takemura, T., and Zhang, H.: Anthropogenic and Natural Radiative Forcing, in: Climate Change 2013: The Physical Science Basis. Contribution of Working Group I to the Fifth Assessment Report of the Intergovernmental Panel on Climate Change, edited by Stocker, T., Qin, D., Plattner, G.-K., Tignor, M., Allen, S., Boschung, J., Nauels, A., Xia, Y., Bex, V., and Midgley, P., chap. 8, pp. 659–740, Cambridge University Press, https://doi.org/10.1017/ CBO9781107415324.018, 2013.

Nisbet, E. G., Dlugokencky, E. J., Manning, M. R., Lowry, D., Fisher, R. E., France, J. L., Michel, S. E., Miller, J. B., White, J. W. C., Vaughn, B., and Others: Rising atmospheric methane: 2007–2014 growth and isotopic shift, Global Biogeochemical Cycles, 30, 1356–1370, 2016.

Nisbet, E. G., Fisher, R. E., Lowry, D., France, J. L., Allen, G., Bakkaloglu, S., Broderick, T. J., Cain, M., Coleman, M., Fernandez, J., Forster, G., Griffiths, P. T., Iverach, C. P., Kelly, B. F. J., Manning, M. R., Nisbet-Jones, P. B. R., Pyle, J. A., Townsend-Small, A., Al-Shalaan, A., Warwick, N., and Zazzeri, G.: Methane Mitigation: Methods to Reduce Emissions, on the Path to the Paris Agreement, Reviews of Geophysics, 58, 1–51, https://doi.org/10.1029/2019rg000675, 2020.

Notholt, J., Petri, C., Warneke, T., Deutscher, N., Buschmann, M., Weinzierl, C., Macatangay, R., and Grupe, P.: TCCON data from Bremen (DE), Release GGG2014R1, TCCON data archive, hosted by CaltechDATA, https://doi.org/10.14291/tccon.ggg2014.bremen01.R1, 2019.

O'Dell, C. W.: Acceleration of multiple-scattering, hyperspectral radiative transfer calculations via low-streams interpolation, Journal of Geophysical Research D: Atmospheres, 115, 1–15, https://doi.org/10.1029/2009JD012803, 2010.

O'Dell, C. W., Connor, B., Bösch, H., O'Brien, D., Frankenberg, C., Castano, R., Christi, M., Eldering, D., Fisher, B., Gunson, M., McDuffie, J., Miller, C. E., Natraj, V., Oyafuso, F., Polonsky, I., Smyth, M., Taylor, T., Toon, G. C., Wennberg, P. O., and Wunch, D.: The ACOS

CO$_{2}$ retrieval algorithm-Part 1: Description and validation against synthetic observations, Atmospheric Measurement Techniques, 5, 99–121, https://doi.org/10.5194/amt-5-99-2012, 2012.

Parker, R. and Boesch, H.: University of Leicester GOSAT Proxy XCH$_4$ v9.0, Centre for Environmental Data Analysis, https://doi.org/10.5285/18ef8247f52a4cb6a14013f8235cc1eb, 2020.

5   Parker, R., Boesch, H., Cogan, A., Fraser, A., Feng, L., Palmer, P. I., Messerschmidt, J., Deutscher, N., Griffith, D. W. T., Notholt, J., Wennberg, P. O., and Wunch, D.: Methane observations from the Greenhouse Gases Observing SATellite: Comparison to ground-based TCCON data and model calculations, Geophysical Research Letters, 38, https://doi.org/10.1029/2011GL047871, 2011.

Parker, R. J., Boesch, H., Byckling, K., Webb, A. J., Palmer, P. I., Feng, L., Bergamaschi, P., Chevallier, F., Notholt, J., Deutscher, N., Warneke, T., Hase, F., Sussmann, R., Kawakami, S., Kivi, R., Griffith, D. W. T., and Velazco, V.: Assessing 5 years of GOSAT Proxy
10   XCH$_4$ data and associated uncertainties, Atmospheric Measurement Techniques, 8, 4785–4801, https://doi.org/10.5194/amt-8-4785-2015, 2015.

Parker, R. J., Boesch, H., Wooster, M. J., Moore, D. P., Webb, A. J., Gaveau, D., and Murdiyarso, D.: Atmospheric CH$_4$ and CO$_2$ enhancements and biomass burning emission ratios derived from satellite observations of the 2015 Indonesian fire plumes, Atmospheric Chemistry and Physics, 16, 10 111–10 131, https://doi.org/10.5194/acp-16-10111-2016, 2016.

15   Parker, R. J., Boesch, H., McNorton, J., Comyn-Platt, E., Gloor, M., Wilson, C., Chipperfield, M. P., Hayman, G. D., and Bloom, A. A.: Evaluating year-to-year anomalies in tropical wetland methane emissions using satellite CH$_4$ observations, Remote Sensing of Environment, 211, 261–275, https://doi.org/10.1016/j.rse.2018.02.011, 2018.

Parker, R. J., Webb, A., Boesch, H., Somkuti, P., Barrio Guillo, R., Di Noia, A., Kalaitzi, N., Anand, J., Bergamaschi, P., Chevallier, F., Palmer, P. I., Feng, L., Deutscher, N. M., Feist, D. G., Griffith, D. W. T., Hase, F., Kivi, R., Morino, I., Notholt, J., Oh, Y.-S., Ohyama,
20   H., Petri, C., Pollard, D. F., Roehl, C., Sha, M. K., Shiomi, K., Strong, K., Sussmann, R., Te, Y., Velazco, V. A., Warneke, T., Wennberg, P. O., and Wunch, D.: A Decade of GOSAT Proxy Satellite CH$_4$ Observations, Earth System Science Data Discussions, 2020, 1–36, https://doi.org/10.5194/essd-2020-114, 2020a.

Parker, R. J., Wilson, C., Bloom, A. A., Comyn-Platt, E., Hayman, G., McNorton, J., Boesch, H., and Chipperfield, M. P.: Exploring Constraints on a Wetland Methane Emission Ensemble (WetCHARTs) using GOSAT Satellite Observations, Biogeosciences Discussions,
25   2020, 1–33, https://doi.org/10.5194/bg-2020-284, 2020b.

Patra, P. K., Houweling, S., Krol, M., Bousquet, P., Belikov, D., Bergmann, D., Bian, H., Cameron-Smith, P., Chipperfield, M. P., Corbin, K., Fortems-Cheiney, A., Fraser, A., Gloor, E., Hess, P., Ito, A., Kawa, S. R., Law, R. M., Loh, Z., Maksyutov, S., Meng, L., Palmer, P. I., Prinn, R. G., Rigby, M., Saito, R., and Wilson, C.: TransCom model simulations of CH$_4$ and related species: linking transport, surface flux and chemical loss with CH$_4$ variability in the troposphere and lower stratosphere, Atmospheric Chemistry and Physics, 11, 12 813–12 837,
30   https://doi.org/10.5194/acp-11-12813-2011, 2011.

Peters, W., Jacobson, A. R., Sweeney, C., Andrews, A. E., Conway, T. J., Masarie, K., Miller, J. B., Bruhwiler, L. M. P., Pétron, G., Hirsch, A. I., Worthy, D. E. J., van der Werf, G. R., Randerson, J. T., Wennberg, P. O., Krol, M. C., and Tans, P. P.: An atmospheric perspective on North American carbon dioxide exchange: CarbonTracker, Proceedings of the National Academy of Sciences, 104, 18 925–18 930, https://doi.org/10.1073/pnas.0708986104, 2007.

35   Pignatti, S., Palombo, A., Pascucci, S., Romano, F., Santini, F., Simoniello, T., Umberto, A., Vincenzo, C., Acito, N., Diani, M., Matteoli, S., Corsini, G., Casa, R., De Bonis, R., Laneve, G., and Ananasso, C.: The PRISMA hyperspectral mission: Science activities and opportunities for agriculture and land monitoring, in: 2013 IEEE International Geoscience and Remote Sensing Symposium - IGARSS, pp. 4558–4561, https://doi.org/10.1109/IGARSS.2013.6723850, 2013.

Pollard, D. F., Sherlock, V., Robinson, J., Deutscher, N. M., Connor, B., and Shiona, H.: The Total Carbon Column Observing Network site description for Lauder, New Zealand, Earth System Science Data, 9, 977–992, https://doi.org/10.5194/essd-9-977-2017, 2017.

Prather, M. J., Holmes, C. D., and Hsu, J.: Reactive greenhouse gas scenarios: Systematic exploration of uncertainties and the role of atmospheric chemistry, Geophysical Research Letters, 39, https://doi.org/10.1029/2012GL051440, 2012.

5 Reuter, M., Buchwitz, M., Schneising, O., Noël, S., Bovensmann, H., Burrows, J. P., Boesch, H., Di Noia, A., Anand, J., Parker, R. J., Somkuti, P., Wu, L., Hasekamp, O. P., Aben, I., Kuze, A., Suto, H., Shiomi, K., Yoshida, Y., Morino, I., Crisp, D., O'Dell, C. W., Notholt, J., Petri, C., Warneke, T., Velazco, V. A., Deutscher, N. M., Griffith, D. W., Kivi, R., Pollard, D. F., Hase, F., Sussmann, R., Té, Y. V., Strong, K., Roche, S., Sha, M. K., De Mazière, M., Feist, D. G., Iraci, L. T., Roehl, C. M., Retscher, C., and Schepers, D.: Ensemble-based satellite-derived carbon dioxide and methane column-averaged dry-air mole fraction data sets (2003-2018) for carbon and climate
10 applications, Atmospheric Measurement Techniques, 13, 789–819, https://doi.org/10.5194/amt-13-789-2020, 2020.

Rigby, M., Prinn, R. G., Fraser, P. J., Simmonds, P. G., Langenfelds, R. L., Huang, J., Cunnold, D. M., Steele, L. P., Krummel, P. B., Weiss, R. F., O'Doherty, S., Salameh, P. K., Wang, H. J., Harth, C. M., Muhle, J., and Porter, L. W.: Renewed growth of atmospheric methane, Geophysical Research Letters, 35, https://doi.org/10.1029/2008GL036037, 2008.

Rigby, M., Montzka, S. A., Prinn, R. G., White, J. W. C., Young, D., O'Doherty, S., Lunt, M. F., Ganesan, A. L., Manning, A. J., Sim-
15 monds, P. G., Salameh, P. K., Harth, C. M., Mühle, J., Weiss, R. F., Fraser, P. J., Steele, L. P., Krummel, P. B., McCulloch, A., Park, S., O'Doherty, S., Lunt, M. F., Ganesan, A. L., Manning, A. J., Simmonds, P. G., Salameh, P. K., Harth, C. M., Mühle, J., Weiss, R. F., Fraser, P. J., Steele, L. P., Krummel, P. B., McCulloch, A., Park, S., O'Doherty, S., Lunt, M. F., Ganesan, A. L., Manning, A. J., Sim-monds, P. G., Salameh, P. K., Harth, C. M., Mühle, J., Weiss, R. F., Fraser, P. J., Steele, L. P., Krummel, P. B., McCulloch, A., and Park, S.: Role of atmospheric oxidation in recent methane growth, Proceedings of the National Academy of Sciences, 114, 5373–5377,
20 https://doi.org/10.1073/pnas.1616426114, 2017.

Rodgers, C. D.: Inverse Methods for Atmospheric Sounding, WORLD SCIENTIFIC, https://doi.org/10.1142/3171, 2000.

Ross, A. N., Wooster, M. J., Boesch, H., and Parker, R.: First satellite measurements of carbon dioxide and methane emission ratios in wildfire plumes, Geophysical Research Letters, 40, 4098–4102, https://doi.org/10.1002/grl.50733, 2013.

Saad, K. M., Wunch, D., Deutscher, N. M., Griffith, D. W. T., Hase, F., De Mazière, M., Notholt, J., Pollard, D. F., Roehl, C. M., Schneider, M.,
25 Sussmann, R., Warneke, T., and Wennberg, P. O.: Seasonal variability of stratospheric methane: implications for constraining tropospheric methane budgets using total column observations, Atmospheric Chemistry and Physics, 16, 14 003–14 024, https://doi.org/10.5194/acp-16-14003-2016, https://acp.copernicus.org/articles/16/14003/2016/, 2016.

Saunois, M., Bousquet, P., Poulter, B., Peregon, A., Ciais, P., Canadell, J. G., Dlugokencky, E. J., Etiope, G., Bastviken, D., Houweling, S., Janssens-Maenhout, G., Tubiello, F. N., Castaldi, S., Jackson, R. B., Alexe, M., Arora, V. K., Beerling, D. J., Bergamaschi, P., Blake, D. R.,
30 Brailsford, G., Brovkin, V., Bruhwiler, L., Crevoisier, C., Crill, P., Covey, K., Curry, C., Frankenberg, C., Gedney, N., Höglund-Isaksson, L., Ishizawa, M., Ito, A., Joos, F., Kim, H.-S., Kleinen, T., Krummel, P., Lamarque, J.-F., Langenfelds, R., Locatelli, R., Machida, T., Maksyutov, S., McDonald, K. C., Marshall, J., Melton, J. R., Morino, I., Naik, V., O'Doherty, S., Parmentier, F.-J. W., Patra, P. K., Peng, C., Peng, S., Peters, G. P., Pison, I., Prigent, C., Prinn, R., Ramonet, M., Riley, W. J., Saito, M., Santini, M., Schroeder, R., Simpson, I. J., Spahni, R., Steele, P., Takizawa, A., Thornton, B. F., Tian, H., Tohjima, Y., Viovy, N., Voulgarakis, A., van Weele, M., van der Werf, G. R.,
35 Weiss, R., Wiedinmyer, C., Wilton, D. J., Wiltshire, A., Worthy, D., Wunch, D., Xu, X., Yoshida, Y., Zhang, B., Zhang, Z., and Zhu, Q.: The global methane budget 2000–2012, Earth System Science Data, 8, 697–751, https://doi.org/10.5194/essd-8-697-2016, 2016.

Saunois, M., Stavert, A. R., Poulter, B., Bousquet, P., Canadell, J. G., Jackson, R. B., Raymond, P. A., Dlugokencky, E. J., Houweling, S., Patra, P. K., Ciais, P., Arora, V. K., Bastviken, D., Bergamaschi, P., Blake, D. R., Brailsford, G., Bruhwiler, L., Carlson, K. M., Carrol,

M., Castaldi, S., Chandra, N., Crevoisier, C., Crill, P. M., Covey, K., Curry, C. L., Etiope, G., Frankenberg, C., Gedney, N., Hegglin, M. I., Höglund-Isaksson, L., Hugelius, G., Ishizawa, M., Ito, A., Janssens-Maenhout, G., Jensen, K. M., Joos, F., Kleinen, T., Krummel, P. B., Langenfelds, R. L., Laruelle, G. G., Liu, L., Machida, T., Maksyutov, S., McDonald, K. C., McNorton, J., Miller, P. A., Melton, J. R., Morino, I., Müller, J., Murguia-Flores, F., Naik, V., Niwa, Y., Noce, S., O'Doherty, S., Parker, R. J., Peng, C., Peng, S., Peters, G. P., Prigent, C., Prinn, R., Ramonet, M., Regnier, P., Riley, W. J., Rosentreter, J. A., Segers, A., Simpson, I. J., Shi, H., Smith, S. J., Steele, L. P., Thornton, B. F., Tian, H., Tohjima, Y., Tubiello, F. N., Tsuruta, A., Viovy, N., Voulgarakis, A., Weber, T. S., van Weele, M., van der Werf, G. R., Weiss, R. F., Worthy, D., Wunch, D., Yin, Y., Yoshida, Y., Zhang, W., Zhang, Z., Zhao, Y., Zheng, B., Zhu, Q., Zhu, Q., and Zhuang, Q.: The Global Methane Budget 2000–2017, Earth System Science Data, 12, 1561–1623, https://doi.org/10.5194/essd-12-1561-2020, 2020.

Schaefer, H., Fletcher, S. E. M., Veidt, C., Lassey, K. R., Brailsford, G. W., Bromley, T. M., Dlugokencky, E. J., Michel, S. E., Miller, J. B., Levin, I., Lowe, D. C., Martin, R. J., Vaughn, B. H., and White, J. W. C.: A 21st-century shift from fossil-fuel to biogenic methane emissions indicated by $^{13}CH_4$, Science, 352, 80–84, https://doi.org/10.1126/science.aad2705, 2016.

Schepers, D., Guerlet, S., Butz, A., Landgraf, J., Frankenberg, C., Hasekamp, O., Blavier, J.-F., Deutscher, N. M., Griffith, D. W. T., Hase, F., Kyro, E., Morino, I., Sherlock, V., Sussmann, R., and Aben, I.: Methane retrievals from Greenhouse Gases Observing Satellite (GOSAT) shortwave infrared measurements: Performance comparison of proxy and physics retrieval algorithms, Journal of Geophysical Research: Atmospheres, 117, https://doi.org/10.1029/2012JD017549, 2012.

Schneising, O., Buchwitz, M., Reuter, M., Bovensmann, H., Burrows, J. P., Borsdorff, T., Deutscher, N. M., Feist, D. G., Griffith, D. W., Hase, F., Hermans, C., Iraci, L. T., Kivi, R., Landgraf, J., Morino, I., Notholt, J., Petri, C., Pollard, D. F., Roche, S., Shiomi, K., Strong, K., Sussmann, R., Velazco, V. A., Warneke, T., and Wunch, D.: A scientific algorithm to simultaneously retrieve carbon monoxide and methane from TROPOMI onboard Sentinel-5 Precursor, Atmospheric Measurement Techniques, 12, 6771–6802, https://doi.org/10.5194/amt-12-6771-2019, 2019.

Sheng, J.-X., Jacob, D. J., Turner, A. J., Maasakkers, J. D., Benmergui, J., Bloom, A. A., Arndt, C., Gautam, R., Zavala-Araiza, D., Boesch, H., and Parker, R. J.: 2010-2015 methane trends over Canada, the United States, and Mexico observed by the GOSAT satellite: contributions from different source sectors, Atmospheric Chemistry and Physics Discussions, pp. 1–18, https://doi.org/10.5194/acp-2017-1110, 2018.

Sherlock, V., Connor, B., Robinson, J., Shiona, H., Smale, D., and Pollard, D.: TCCON data from Lauder (NZ), Release GGG2014R0, TCCON Data Archive, hosted by CaltechDATA, https://doi.org/10.14291/tccon.ggg2014.lauder01.R0/1149293, 2014a.

Sherlock, V., Connor, B., Robinson, J., Shiona, H., Smale, D., and Pollard, D.: TCCON data from Lauder (NZ), Release GGG2014R0, TCCON data archive, hosted by CaltechDATA, https://doi.org/10.14291/tccon.ggg2014.lauder02.R0/1149298, 2014b.

Shiomi, K., Kawakami, S., Ohyama, H., Arai, K., Okumura, H., Taura, C., Fukamachi, T., and Sakashita, M.: TCCON data from Saga (JP), Release GGG2014.R0, TCCON Data Archive, hosted by CaltechDATA, https://doi.org/10.14291/tccon.ggg2014.saga01.R0/114928, 2014.

Siddans, R., Knappett, D., Kerridge, B., Waterfall, A., Hurley, J., Latter, B., Boesch, H., and Parker, R.: Global height-resolved methane retrievals from the Infrared Atmospheric Sounding Interferometer (IASI) on MetOp, Atmospheric Measurement Techniques, https://doi.org/10.5194/amt-10-4135-2017, 2017.

Stanevich, I., Jones, D. B. A., Strong, K., Keller, M., Henze, D. K., Parker, R. J., Boesch, H., Wunch, D., Notholt, J., Petri, C., Warneke, T., Sussmann, R., Schneider, M., Hase, F., Kivi, R., Deutscher, N. M., Velazco, V. A., Walker, K. A., and Deng, F.: Characterizing model errors in chemical transport modelling of methane: Using GOSAT XCH$_4$ data with weak constraint four-dimensional variational data assimilation, Atmospheric Chemistry and Physics Discussions, 2019, 1–54, https://doi.org/10.5194/acp-2019-786, 2019.

Stanevich, I., Jones, D. B. A., Strong, K., Parker, R. J., Boesch, H., Wunch, D., Notholt, J., Petri, C., Warneke, T., Sussmann, R., Schneider, M., Hase, F., Kivi, R., Deutscher, N. M., Velazco, V. A., Walker, K. A., and Deng, F.: Characterizing model errors in chemical transport modeling of methane: impact of model resolution in versions v9-02 of GEOS-Chem and v35j of its adjoint model, Geoscientific Model Development, 13, 3839–3862, https://doi.org/10.5194/gmd-13-3839-2020, 2020.

5 Strong, K., Roche, S., Franklin, J. E., Mendonca, J., Lutsch, E., Weaver, D., Fogal, P. F., Drummond, J. R., Batchelor, R., and Lindenmaier, R.: TCCON data from Eureka (CA), Release GGG2014R3, TCCON data archive, hosted by CaltechDATA, https://doi.org/10.14291/tccon.ggg2014.eureka01.R3, 2019.

Sussmann, R. and Rettinger, M.: TCCON data from Garmisch (DE), Release GGG2014R2, TCCON Data Archive, hosted by CaltechDATA, https://doi.org/10.14291/tccon.ggg2014.garmisch01.R2, 2018.

10 Suto, H., Kataoka, F., Kikuchi, N., Knuteson, R. O., Butz, A., Haun, M., Buijs, H., Shiomi, K., Imai, H., and Kuze, A.: Thermal and near-infrared sensor for carbon observation Fourier-transform spectrometer-2 (TANSO-FTS-2) on the Greenhouse Gases Observing Satellite-2 (GOSAT-2) during its first year on orbit, Atmospheric Measurement Techniques Discussions, 2020, 1–51, https://doi.org/10.5194/amt-2020-360, 2020.

Té, Y., Jeseck, P., and Janssen, C.: TCCON data from Paris (FR), Release GGG2014.R0, TCCON Data Archive, hosted by CaltechDATA,
15 https://doi.org/10.14291/tccon.ggg2014.paris01.R0/1149279, 2014.

Toon, G. C.: Atmospheric Line List for the 2014 TCCON Data Release, https://doi.org/10.14291/TCCON.GGG2014.ATM.R0/1221656, https://data.caltech.edu/records/248, 2015.

Tunnicliffe, R. L., Ganesan, A. L., Parker, R. J., Boesch, H., Gedney, N., Poulter, B., Zhang, Z., Lavrič, J. V., Walter, D., Rigby, M., Henne, S., Young, D., and O'Doherty, S.: Quantifying sources of Brazil's CH_4 emissions between 2010 and 2018 from satellite data, Atmospheric
20 Chemistry and Physics Discussions, 2020, 1–40, https://doi.org/10.5194/acp-2020-438, 2020.

Turner, A. J., Jacob, D. J., Wecht, K. J., Maasakkers, J. D., Lundgren, E., Andrews, A. E., Biraud, S. C., Boesch, H., Bowman, K. W., Deutscher, N. M., Dubey, M. K., Griffith, D. W. T., Hase, F., Kuze, A., Notholt, J., Ohyama, H., Parker, R., Payne, V. H., Sussmann, R., Sweeney, C., Velazco, V. A., Warneke, T., Wennberg, P. O., and Wunch, D.: Estimating global and North American methane emissions with high spatial resolution using GOSAT satellite data, Atmospheric Chemistry and Physics, 15, 7049–7069, https://doi.org/10.5194/acp-
25 15-7049-2015, 2015.

Turner, A. J., Frankenberg, C., Wennberg, P. O., and Jacob, D. J.: Ambiguity in the causes for decadal trends in atmospheric methane and hydroxyl, Proceedings of the National Academy of Sciences, 114, 5367–5372, https://doi.org/10.1073/pnas.1616020114, 2017.

Velazco, V. A., Morino, I., Uchino, O., Hori, A., Kiel, M., Bukosa, B., Deutscher, N. M., Sakai, T., Nagai, T., Bagtasa, G., Izumi, T., Yoshida, Y., and Griffith, D. W.: TCCON Philippines: First measurement results, satellite data and model comparisons in Southeast Asia, Remote
30 Sensing, 9, 1–18, https://doi.org/10.3390/rs9121228, 2017.

Wang, Z., Warneke, T., Deutscher, N. M., Notholt, J., Karstens, U., Saunois, M., Schneider, M., Sussmann, R., Sembhi, H., Griffith, D. W., Pollard, D. F., Kivi, R., Petri, C., Velazco, V. A., Ramonet, M., and Chen, H.: Contributions of the troposphere and stratosphere to CH_4 model biases, Atmospheric Chemistry and Physics, 17, 13 283–13 295, https://doi.org/10.5194/acp-17-13283-2017, 2017.

Warneke, T., Messerschmidt, J., Notholt, J., Weinzierl, C., Deutscher, N. M., Petri, C., Grupe, P., Vuillemin, C., Truong, F., Schmidt, M., Ra-
35 monet, M., and Parmentier, E.: TCCON data from Orléans (FR), Release GGG2014.R0, TCCON Data Archive, hosted by CaltechDATA, https://doi.org/10.14291/tccon.ggg2014.orleans01.R0/1149276, 2014.

Webb, A. J., Bösch, H., Parker, R. J., Gatti, L. V., Gloor, E., Palmer, P. I., Basso, L. S., Chipperfield, M. P., Correia, C. S. C., Domingues, L. G., Feng, L., Gonzi, S., Miller, J. B., Warneke, T., and Wilson, C.: CH_4 concentrations over the Amazon from GOSAT consistent with in situ vertical profile data, Journal of Geophysical Research: Atmospheres, 121, 6–11,11,20, https://doi.org/10.1002/2016JD025263, 2016.

Wecht, K. J., Jacob, D. J., Sulprizio, M. P., Santoni, G. W., Wofsy, S. C., Parker, R., Bösch, H., and Worden, J.: Spatially resolving methane emissions in California: Constraints from the CalNex aircraft campaign and from present (GOSAT, TES) and future (TROPOMI, geostationary) satellite observations, Atmospheric Chemistry and Physics, 14, 4119–4148, https://doi.org/10.5194/acp-14-8173-2014, 2014.

Wennberg, P. O., Wunch, D., Roehl, C., Blavier, J.-F., Toon, G. C., Allen, N., Dowell, P., Teske, K., Martin, C., and Martin, J.: TCCON data from Lamont (US), Release GGG2014.R1, TCCON Data Archive, hosted by CaltechDATA, https://doi.org/10.14291/tccon.ggg2014.lamont01.R1/1255070, 2016.

Wennberg, P. O., Roehl, C., Wunch, D., Toon, G. C., Blavier, J. F., Washenfelder, R., Keppel-Aleks, G., Allen, N., and Ayers, J.: TCCON data from Park Falls (USA), Release GGG2014R1, TCCON data archive, hosted by CaltechDATA, https://doi.org/10.14291/tccon.ggg2014.parkfalls01.R1, 2017.

Worden, J. R., Turner, A. J., Bloom, A., Kulawik, S. S., Liu, J., Lee, M., Weidner, R., Bowman, K., Frankenberg, C., Parker, R., and Payne, V. H.: Quantifying lower tropospheric methane concentrations using GOSAT near-IR and TES thermal IR measurements, Atmospheric Measurement Techniques, 8, 3433–3445, https://doi.org/10.5194/amt-8-3433-2015, 2015.

Worden, J. R., Bloom, A. A., Pandey, S., Jiang, Z., Worden, H. M., Walker, T. W., Houweling, S., and Röckmann, T.: Reduced biomass burning emissions reconcile conflicting estimates of the post-2006 atmospheric methane budget, Nature Communications, 8, 1–11, https://doi.org/10.1038/s41467-017-02246-0, 2017.

Wunch, D., Toon, G. C., Wennberg, P. O., Wofsy, S. C., Stephens, B. B., Fischer, M. L., Uchino, O., Abshire, J. B., Bernath, P., Biraud, S. C., Blavier, J.-F. L., Boone, C., Bowman, K. P., Browell, E. V., Campos, T., Connor, B. J., Daube, B. C., Deutscher, N. M., Diao, M., Elkins, J. W., Gerbig, C., Gottlieb, E., Griffith, D. W. T., Hurst, D. F., Jiménez, R., Keppel-Aleks, G., Kort, E. A., Macatangay, R., Machida, T., Matsueda, H., Moore, F., Morino, I., Park, S., Robinson, J., Roehl, C. M., Sawa, Y., Sherlock, V., Sweeney, C., Tanaka, T., and Zondlo, M. A.: Calibration of the Total Carbon Column Observing Network using aircraft profile data, Atmospheric Measurement Techniques, 3, 1351–1362, https://doi.org/10.5194/amt-3-1351-2010, 2010.

Wunch, D., Toon, G. C., Blavier, J.-F. L., Washenfelder, R. A., Notholt, J., Connor, B. J., Griffith, D. W. T., Sherlock, V., and Wennberg, P. O.: The Total Carbon Column Observing Network, Philosophical Transactions of the Royal Society of London A: Mathematical, Physical and Engineering Sciences, 369, 2087–2112, https://doi.org/10.1098/rsta.2010.0240, 2011.

Wunch, D., Mendonca, J., Colebatch, O., Allen, N., Blavier, J.-F. L., Roche, S., Hedelius, J., Neufeld, G., Springett, S., Worthy, D., Kessler, R., and Strong, K.: TCCON data from East Trout Lake (CA), Release GGG2014.R1, TCCON Data Archive, hosted by CaltechDATA, https://doi.org/10.14291/tccon.ggg2014.easttroutlake01.R1, 2018.

Yin, Y., Chevallier, F., Ciais, P., Bousquet, P., Saunois, M., Zheng, B., Worden, J., Bloom, A. A., Parker, R., Jacob, D., Dlugokencky, E. J., and Frankenberg, C.: Accelerating methane growth rate from 2010 to 2017: leading contributions from the tropics and East Asia, Atmospheric Chemistry and Physics Discussions, 2020, 1–27, https://doi.org/10.5194/acp-2020-649, 2020.

Yoshida, Y., Kikuchi, N., Morino, I., Uchino, O., Oshchepkov, S., Bril, A., Saeki, T., Schutgens, N., Toon, G. C., Wunch, D., Roehl, C. M., Wennberg, P. O., Griffith, D. W., Deutscher, N. M., Warneke, T., Notholt, J., Robinson, J., Sherlock, V., Connor, B., Rettinger, M., Sussmann, R., Ahonen, P., Heikkinen, P., Kyrö, E., Mendonca, J., Strong, K., Hase, F., Dohe, S., and Yokota, T.: Improvement of the retrieval algorithm for GOSAT SWIR XCO_2 and XCH_4 and their validation using TCCON data, Atmospheric Measurement Techniques, 6, 1533–1547, https://doi.org/10.5194/amt-6-1533-2013, 2013.

Zhang, Y., Jacob, D. J., Lu, X., Maasakkers, J. D., Scarpelli, T. R., Sheng, J.-X., Shen, L., Qu, Z., Sulprizio, M. P., Chang, J., Bloom, A. A., Ma, S., Worden, J., Parker, R. J., and Boesch, H.: Attribution of the accelerating increase in atmospheric methane during 2010–2018 by inverse analysis of GOSAT observations, Atmospheric Chemistry and Physics Discussions, 2020, 1–42, https://doi.org/10.5194/acp-2020-964, 2020.

5   Zheng, B., Chevallier, F., Yin, Y., Ciais, P., Fortems-Cheiney, A., Deeter, M. N., Parker, R. J., Wang, Y., Worden, H. M., and Zhao, Y.: Global atmospheric carbon monoxide budget 2000–2017 inferred from multi-species atmospheric inversions, Earth System Science Data, 11, 1411–1436, https://doi.org/10.5194/essd-11-1411-2019, 2019.